Processing, Microstructure and Properties of Hybrid Metallic and Ceramic Reinforced Aluminium Composites

A thesis submitted in partial fulfillment of the requirements for the degree of

Master of Technology

in

Metallurgical and Materials Engineering

by

Shanta Mohapatra
(Roll No- 210MM1250)

Department of Metallurgical and Materials Engineering
National Institute Of Technology, Rourkela
2013

Processing, Microstructure and Properties of Hybrid Metallic and Ceramic Reinforced Aluminium Composites

A thesis submitted in partial fulfillment of the requirements for the degree of

Master of Technology

in

Metallurgical and Materials Engineering

by

Shanta Mohapatra

Under the guidance and supervision of

Prof. Ashok Kumar Mondal

Department of Metallurgical and Materials Engineering

National Institute Of Technology, Rourkela
2013

National Institute Of Technology
Rourkela

CERTIFICATE

This is to certify that the thesis entitled, "**Processing, Microstructure and Properties of Hybrid Metallic and Ceramic Reinforced Aluminium Composites"** submitted by **Shanta Mohapatra(211MM1363)** in partial fulfillment of the requirements for the award of Master of Technology in **Metallurgical and Materials Engineering** at the National Institute of Technology, Rourkela is a bonafide research work carried out by her under my supervision and guidance.

To the best of my knowledge, the matter embodied in the thesis is based on candidate's own work, has not been submitted to any other university / institute for the award of any degree or diploma.

Date:

Supervisor

Prof. Ashok Kumar Mondal
Dept. of Metallurgical and Materials Engg.
National Institute of Technology
Rourkela – 769008

Acknowledgement

I take this opportunity to owe many thanks to the Department of Metallurgical and Materials Engineering, National Institute of Technology Rourkela for offering a unique platform to earn exposure and garner knowledge.

I wish to extend my sincere and heartfelt gratitude to my guide Prof. A. K. Mondal, a true guide who supported and encouraged me during the entire tenure of the project. He inspired me to drive this thesis towards the path of glory and success.

I also thank to Prof. B. C. Ray, the HOD, Department of Metallurgical and Materials Engineering, National Institute of Technology Rourkela for granting me permission to do this project and avail all the facilities in the department. I also express my thanks to all other Professors of our department for their co-operation and valuable advice during the course work and my project work.

I am grateful and thankful to the technical assistants Mr. U. K Sahu, Mr. S. Hemram, Mr. A. Pal and Mr. S. Pradhan for the support they rendered during the execution of my project. I will never forget to mention some of my seniors like Mr. Anil Kumar Singh Bankoti, Miss. Pankajini Samal, Mrs. Sanghamitra Sethi and Mr. Rajan Kumar Behera who helped me with multiple ideas during completion of my thesis.

There are many who I may have left out in the acknowledgement, but whose co-operation no doubt went a long way in completing this project in time.

Shanta Mohapatra

Abstract

In the present investigation, the combined Ti (micro) and Al_2O_3 (micro or nano) particles reinforced commercially pure Al matrix composites have been developed via powder metallurgy route. A detailed microstructural characterization and the evaluation of mechanical properties including wear and corrosion behaviour have been carried out. As a basis for comparison, the same has been investigated for the Al composites reinforced with these particles alone. The various combinations were Al+8%Ti (Al+Ti), Al+8%micro-Al_2O_3 (Al+MA), Al+8%nano-Al_2O_3 (Al+NA), Al+8%Ti+8%micro-Al_2O_3 (Al+Ti+MA) and Al+8%Ti+8%nano-Al_2O_3 (Al+Ti+MA) (all vol.%).

Microstructural characterization revealed that there is no nano-Al_2O_3 particles agglomeration in the composites. The interfacial integrity between the matrix and the reinforcements was good. The Al+NA and Al+Ti+NA composites exhibited significant grain refinement following the addition of nano-sized Al_2O_3 particles. This might be due to the presence of relatively harder Al_2O_3 particles that inhibits grain growth. The composites reinforced with the ceramic particles (micro or nano) alone exhibited higher hardness values as compared to the composite reinforced with metallic particles alone. In addition, the composites reinforced with the nano-sized Al_2O_3 particles alone exhibited higher hardness value as compared to the composite reinforced with the micro-sized Al_2O_3 particles alone. Further the hybrid composites Al+Ti+MA and Al+Ti+NA exhibited a relatively higher hardness values and the same was higher for the later composite. The increase in hardness might be owing to the grain refinement observed in the Al+NA and Al+Ti+NA composites. The stress values sustained by all the composites specimens in compression tests during 50% reduction of their initial height exhibited a similar trend as hardness. Wear tests were conducted on a pin-on-disc set-up under dry sliding condition using a constant sliding velocity of 1.57 m/s for a

constant sliding distance of 1.0 km and at a load of 30 N. It is observed that the hybrid composites exhibit a better wear resistance than the composite reinforced with individuals particles owing to their higher hardness as compared to that of the other composites. The dominant wear mechanism is observed to be delamination for the Al+Ti composite and abrasion for the rest of the composites. The short term and long term corrosion behaviour was evaluated by electrochemical corrosion tests. It is observed that the Al+Ti composite exhibited the lowest corrosion rate. The composites reinforced with the ceramic particles alone exhibited higher corrosion rate as compared to the Al+Ti composite. In addition, the Al+NA composites exhibited better corrosion resistance as compared to the Al+MA composite. Further relatively higher corrosion rates were exhibited by the hybrid composites. Again the Al+Ti+NA exhibited superior corrosion resistance as compared to that of the Al+Ti+MA. The same was also confirmed by the long term electrochemical impedance spectroscopy (EIS) studies. It was observed that the film on the Al+Ti composite was thin, uniform and obviously dense whereas the other composites exhibited thick but irregular and loose films. The surface of the composite Al+Ti+MA appears to be most degraded than that of the other composites. The discontinuous corroded film with a large size of pits was noted on the surface of it. However, the film is relatively continuous and less number of small sized pits is present on the corroded surfaces of other composites. The observed grain refinement in the Al+NA and Al+Ti+NA composites might have contributed to the improved corrosion resistance. Furthermore, the particles can be considered as defects in the passive film. Thus, it is difficult to build a dense passive layer free from defects in case of the composites reinforced with higher volume fraction of ceramic and metallic particles. All the above features are detrimental and may cause difference in corrosion resistance among the composites although it is not possible to separate them.

Contents

Chapter 1: Introduction……..1-3

1.1. Introduction ……...2-3

Chapter 2: Literature review……...4-16

2.1. Metal Matrix Composites (MMCs) ……..5

2.1.1. Definition and importance of MMCs……..5

2.1.2. Reinforcements for MMCs……..5-6

2.1.3. Fabrication routes for MMCs……..6-7

2.1.4. Importance of interface in MMCs……...7

2.2. Definitions of properties……8-9

2.2.1. Hardness……..8

2.2.2. Wear……....9

2.3. Summary of relevant literatures……10-16

2.3.1. MMCs reinforced with metallic particles……10-13

2.3.2. MMCs reinforced with nano ceramic particles ……...13-14

2.3.3. MMCs reinforced with both micro and nano ceramic particles……..14-15

2.3.4. MMCs reinforced with both metallic and ceramics particles……..15-16

Chapter 3: Materials and experimental procedure……17-23

3.1 Specimen fabrication……18

3.1.1. Raw materials……18

3.1.2. Blending……18

3.1.3. Compaction……..18-19

3.1.4. Sintering……19

3.2. Specimen characterization……..19

3.2.1. XRD analysis……..19

3.2.2. Scanning Electron Microscopy (SEM) observation…….....19-20

3.3.1. Density measurement……20

3.4.1. Hardness measurement……...20

3.4.2. Wear tests……..20-21

3.4.3. Compression tests……...21
3.4.4. Corrosion tests……..22-23

Chapter 4: Results and discussion……24-48

4.1. Synthesis……..25
4.2. Density and porosity……..25-26
4.3. XRD analysis……26-27
4.4. Microstructure……27-30
4.5. Microhardness……30-31
4.6. Compression strength……31-32
4.7. Dry sliding wear behavior……..33-38
4.7.1. Wear rate……..33-34
4.7.2. Observation of the worn surfaces……34-36
4.7.3. Reason for the difference in wear behavior……36-38
4.8. Electro-chemical corrosion behavior……38-47
4.8.1. Nature of the corrosion response **……38-44**
4.8.2. Morphology of the corroded surfaces……..45-46
4.8.3. Reasons for the difference in corrosion behavior……47

Chapter 5: Conclusions……...48-50

References……51-53

List of figures

Figure number	Figure description	Page number
Fig 2.1	Steps involved in nano-Indentation during Vicker's Hardness test.	8
Fig 3.1	Load application during uni-axial compression test.	21
Fig 4.1	X-ray diffraction patterns obtained from all the Al-based composites.	27
Fig 4.2	Representative as sintered SEM micrographs for all the Al-based composites corresponding to: (a) Al+Ti; (b)Al+NA; (c) Al+MA; (d) Al+Ti+NA; (e) Al+Ti+MA and (f) Al-Ti binary phase diagram.	27-28
Fig 4.3	SEM micrograph (in BSE mode) of the composite Al+NA showing minimum agglomeration of nano-Al_2O_3 particles.	30
Fig 4.4	Variation of the average microhardness values for all the Al-based composites.	30
Fig 4.5	Comparison of the stress values withstand at 50% reduction of the composites specimens	32
Fig 4.6	Variation of the volumetric wear rate for the Al-based composites tested using 30 N load and sliding speed of 1.5 m/s.	33
Fig 4.7	SEM micrographs of the worn surfaces corresponding to the (a) Al+Ti;(b) Al+MA; (c) Al+NA; (d) Al+Ti+MA; (e) Al+Ti+NA and (e) Magnified view of (a).	34-35
Fig 4.8	Variation of open circuit potential for all the Al-based composites.	39
Fig 4.9	Average values of the open circuit potential for all the Al-based composites.	39

Fig 4.10	Variation of the corrosion rates calculated from the potentio dynamic polarization plots for all the Al-based composites.	40
Fig 4.11	Nyquist plots for all the composites after (a) 3 hrs (b) 6 hrs (c) 9 hrs (d) 12 hrs (e) 15 hrs and (f) 18 hrs of immersion.	42-44
Fig 4.12	SEM micrographs of the corroded surfaces corresponding to the (a) Al+Ti; (b) Al+MA; (c) Al+NA; (d) Al+Ti+MA; (e) Al+Ti+NA.	45-46

List of tables

Table number	Description	Page number
Table 2.1	Trends in costs for different processes and reinforcements.	**7**
Table 3.1	Various combinations of the Ti and Al_2O_3 particles in the composites and their corresponding abbreviated nomenclature.	**18**
Table 4.1	Results of density and porosity measurements for the Al-based composites	**26**

Chapter 1

Introduction

1.1. Introduction

Al and Al alloys became attractive candidate for the application in aerospace, defence and automotive industries owing to their versatile properties. A major requirement for such applications is the high strength along with reasonable ductility. There has been a constant effort to enhance the mechanical properties of Al alloys by alloying additions, heat treatment, thermo-mechanical processing, severe plastic deformation (SPD) and so on. However, these methods have their own limitations which are difficult to overcome. For example, many SPD processes produce relatively small quantities of material and therefore, it is very difficult to produce large quantities of materials at low cost. The development of the metal matrix composites (MMCs) is a well-accepted method to improve the strength of metals and alloys. In the race for production of MMCs, aluminium metal matrix composites (AMMCs) received particular attention in the automobile and aerospace industries as potential advanced structural materials in the past three decades owing to their high specific strength, stiffness, superior wear resistance, excellent elevated temperature resistance and the widespread availability of the low cost fabrication techniques [1-5]. The continuous fibre reinforced AMMCs are ruled out owing to their high cost, the whiskers are not preferred due to health hazards and the short fibre reinforced AMMCs exhibit anisotropic properties. Therefore, the Al based particles reinforced composites having low density, good formability and isotropic properties have to be developed. The AMMCs reinforced with the popular ceramic particles like SiC, Al_2O_3, TiO_2, AlN, B_4C and TiC [6] exhibit the beneficial effect of superior strength, however, suffer from the serious disadvantage of low ductility [7-10]. The reduction in ductility arises owing to the brittle interfacial reaction products, poor wettability, particle clusters as well as the presence of porosity and de-bonding at the particle–matrix interface. There have been a few recent investigations on the composites reinforced with hard metallic particles [11-17] that exhibited reasonable good ductility. Therefore, an alternative approach

in the step of designing composites would be to take the simultaneous advantage of ductility from the addition of metallic reinforcement as well as the strength from the addition of hard ceramic particles. The composites reinforced with both metallic as well as ceramic particles are expected to exhibit a good combination of strength and ductility.

Titanium is an attractive choice as reinforcement owing to its high specific strength, high stiffness, good fatigue properties, good creep and high temperature oxidation resistance [12]. In the present investigation, Ti particles (macro) and Al_2O_3 particles (macro and nano) reinforced Al matrix composite have been processed via powder metallurgy route. A detailed microstructural as well as mechanical, wear and corrosion characterizations have been carried out.

Chapter 2

Literature review

2.1. Metal Matrix Composites (MMCs):

2.1.1. Definition and importance of MMCs:

The advantage of utilizing the beneficial properties of the constituent materials, to satisfy the specific demands, is the driving force for the development of composites. In this thesis, our focus will be on the metal matrix composites (MMCs) and more specifically on the aluminium metal matrix composites (AMMCs). The emergence of MMCs as a distinct technology can be traced back to late 1970's when there was an immediate requirement for improved military system. However, it was only in 80's that an impressive effort was made for the research and development on MMCs [18].

As a brief description, AMMCs consist of aluminium as the matrix. Generally reinforcements used in this case are ceramics such as SiC, Al_2O_3, TiO_2, AlN, B_4C, TiC and so on [19]. However, recently there been some work reported on the metallic reinforcements as well [20, 21]. The AMMCs received particular attention in the automobile and aerospace industries as potential advanced structural materials in the past three decades owing to their

- High specific strength
- Improved stiffness
- Reduced density
- Improved high temperature properties (creep, oxidation, corrosion)
- Control thermal expansion coefficient
- Improved abrasion and wear resistance

2.1.2. Reinforcements used for MMCs:

Ceramic particles, mainly SiC and Al_2O_3, are some of the most widely used materials for reinforcing the Al and Al alloys [22]. The SiC possesses some important characteristics like

low cost, easy availability, improves wear behaviour, and promotes an increase in the Young's modulus and tensile strength of the composite. On the other hand, Al_2O_3 is more stable and inert and has better corrosion and high temperature behaviour [23,24]. Recently lots of research is being carried out on the incorporation of metallics/intermetallics as reinforcements [25]. It was observed that the metallics/intermetallics improve wear and corrosion resistance as well as the mechanical properties [26]. It has also got advantages of its high ductility, high wettability and high compatibility with the matrix as compared with ceramics [27]. The reinforcements may be of different types: particles, whiskers, long and short fibers. The long fibre is quite expensive and therefore not suitable from economic point of view. The short fibres are also costly and it exhibits anisotropic properties. Whiskers are becoming outdated owing to health hazards. On the other hand, particles are of less cost and show isotropic properties [22]. A comparison on the cost involved with different reinforcements is shown in Table 2.1. The incorporation of different types of fibres and/or particles into a single matrix has led to the development of hybrid composites. The advantage of using a hybrid composite is that one type of reinforcement could complement with what are lacking in the other. As a result, a balance in cost and performance can be achieved in hybrid composites.

2.1.3. Fabrication routes for MMCs:

There are various routes available for the fabrication of MMCs. These are diffusion joining, powder metallurgy, spray methods, melting process and so on. In this present study, the composites are synthesized by powder metallurgy (P/M) route. It offers some advantages, the main of which is the low manufacturing temperature thus reducing undesired reactions between the matrix and the reinforcement. In addition, it is easier to incorporate particles as

reinforcement by P/M than any other alternative routes [28]. Another advantage of P/M is the uniformity in the reinforcement distribution. This uniformity not only improves the structural properties but also the reproducibility of the properties [28]. A comparison on the cost involved with different fabrication routes is shown in Table 2.1.

Table 2.1: Trends in costs for different fabrication routes and reinforcements

Process	Cost	Reinforcement
Diffusion joining		Monofilaments
Powder metallurgy		Whiskers
Spray methods		Short fibers
Melting process		Particles

2.1.4. Importance of interface in MMCs:

The interface between the matrix and the secondary reinforcing phase plays a vital role in the performance of composite materials. Sometimes the reaction product proves to be detrimental to hamper the properties of the composite. In order to avoid such a situation, we need to concentrate on two important features namely the chemical reactions and the strength of bonding. The composition of the matrix and the reinforcement predicts the interfacial reaction that takes place. The porosity and surface cleanliness can also affect to some extent. The strength of a composite is greatly affected by the orientation and distribution of the reinforcements in the matrix.

2.2. Definition of properties:

2.2.1. Hardness:

Hardness is the property of a material by virtue of which the material resists to plastic deformation. There are various types of hardness test, but we will consider the one where hardness is measured by indentation and more specifically the Vickers' Hardness test. The indenter is a diamond and in the form of a square based pyramid whose opposite sides meet at 136°. The load is fixed and the indenter is pressed into the surface. After a dwelt time, the load is removed. And then the size of the residual indent is measured under a calibrated microscope since it is too small (usually no more than 0.5 mm) to be seen in naked eyes It is determined by measuring the two diagonals of the pyramid of the indentation. The hardness is measured by the formula:

$$HV = [2F \sin (136°/2]/d^2$$

$$HV = 1.854\ F/d^2$$

Given a fixed load and a specific indenter, the smaller the indentation is, the harder the material is.

.

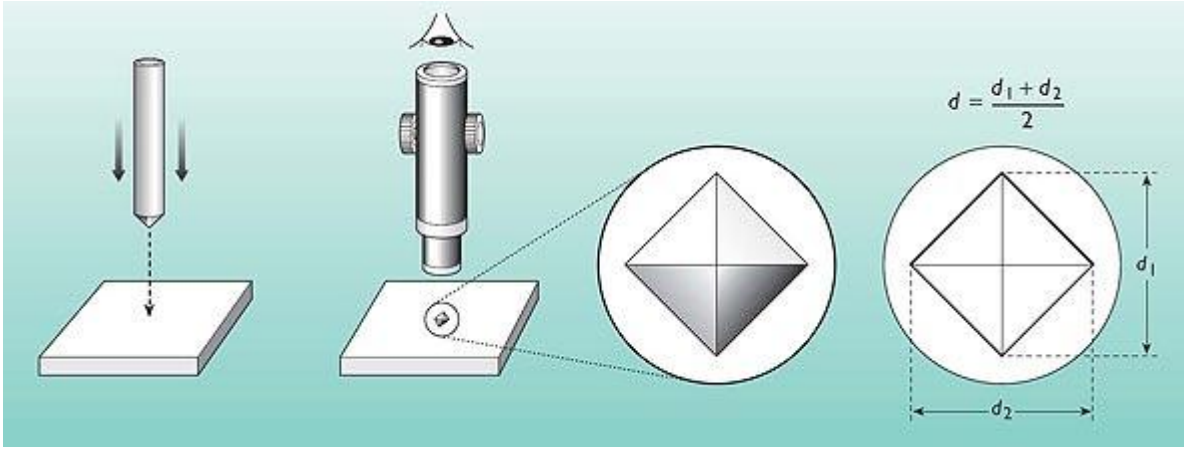

Fig 2.1: Steps involved in nano-Indentation during Vicker's Hardness test.

2.2.2. Wear:

Wear is defined as the removal of the material from the surface of a solid body as a result of mechanical action of the counter body. Wear can be of many types like : Abrasive wear, Adhesive wear, Fatigue wear, Corrosive wear, Erosive wear. Our present study will emphasize on abrasive wear. This occurs when a hard surface slides over a soft surface. The asperities are intentionally provided on the surfaces to add friction so that one surface can move relative to the other. But, these asperities on the harder material cause wear in the other one. If there is involvement of only two surfaces, the wear in this case is called two-body wear. And, if the wear takes place due to a hard particle (grit) trapped in between the rubbing surfaces then it is a three-body abrasive wear. The consequence of the abrasion can be one of the following wear modes: Ploughing, Cutting and Fragmentation. Ploughing takes place when the material is not removed from the surface; rather it moves to a side of the grooves formed. But in Cutting, the materials get separated from the surface and the volume of material loss is equal to the volume of the wear groove. When the removal of materials takes place along with the formation of cracks in the subsurface regions around the wear groove, then the process is called Fragmentation. Adhesive wear, as the name suggests, is caused by the formation of micro-joints due to welding at the point of contact of the two rubbing surfaces. As the load increases, rupture takes place at the micro-joints and some material of one surface is carried away by the other surface. Fatigue wear of the materials takes place when it subjected to cyclic loading when friction exists. In this case, cracks start at the material surface and spread to the subsurface regions. The cracks may connect to each other resulting in separation and delamination of the material pieces. Erosive wear is caused by the impact of particles of solid or liquid against the surface of an object, whereas Corrosion wear takes place due to the devastating effect of the corrosive atmosphere.

2.3. Summary of relevant literatures

2.3.1. MMCs reinforced with metallic particles:

Hassan and Gupta investigated the elemental titanium particle reinforced magnesium synthesized using disintegrated melt deposition technique followed by hot extrusion. They concluded that the addition of titanium as reinforcement marginally improves the dimensional stability of pure magnesium. The presence of titanium reinforcement led to an improvement of 0.2% yield strength and ductility while the UTS were adversely affected. They observed the particle breakage was the dominating reinforcement-associated failure mechanism under tensile loading [29]. Hassan and Gupta in another investigation synthesized the elemental Ni reinforced Mg using an innovative disintegrated melt deposition technique followed by hot extrusion. Microstructural characterization of the composite showed uniform distribution of Ni particles in the matrix, good interfacial integrity of magnesium matrix with nickel particles and Mg-Ni based intermetallics, and the presence of minimal porosity. Physical properties characterization revealed that addition of nickel as reinforcement improves the dimensional stability of pure magnesium. Mechanical properties characterization revealed that the presence of nickel reinforcement lead to significant improvement in hardness, elastic modulus, 0.2% yield strength and UTS while the ductility was adversely affected. The results further revealed that the combination of0.2% yield strength, UTS, and ductility exhibited by nickel reinforced magnesium remained much superior even when compared to high strength magnesium alloy AZ91 reinforced with much higher volume percentage of SiC [30]. Wong et al. [31] reported the successful processing of nano-sized Cu particles reinforced Al composites using powder metallurgy technique incorporating microwave assisted two-directional sintering. The sintered specimens were hot extruded and characterized in terms of physical, microstructural and mechanical properties. Microstructural characterization revealed minimal porosity and the presence of a continuous

network of nano-size Cu particles and Mg_2Cu intermetallic phase decorating\the particle boundaries of the metal matrix. Coefficient of thermal expansion value of magnesium matrix was improved marginally with the addition of nano-size Cu particles. The addition of nano-size Cu particles lead to an increase in hardness, elastic modulus, 0.2% yield strength (YS), ultimate tensile strength (UTS) and work of fracture of the matrix [31]. Thakur and Gupta first developed the Al based composite reinforced with Ti particles fabricated by using the disintegrated melt deposition (DMD) processing technique followed by hot extrusion. Microstructural characterization of the as-extruded composite samples revealed a near uniform distribution of the Ti particles in the Al matrix, good interfacial integrity between the Ti particles and the Al matrix and minimal presence of porosity. The addition of Ti particles resulted in an increase in macrohardness, 0.2% YS, UTS and elastic modulus. However, the ductility of the composite was found to be decreased by the addition of Ti particles in the Al matrix. The fractured samples of the composite showed the ductile mode of fracture in the case of Al matrix whilst particle fracture and debonding were observed as the failure mode of the Ti reinforcement [32]. An experimental analysis was performed to predict flow curves, dynamic recrystallisation behaviour of AZ91magnesium/titanium metal matrix composite based on result from hot compression test. The compression tests were carried out in a temperature range of 300°–500°C and at a strain rate range of 0.001–1 sec^{-1} and the flow curves were obtained. The processing map of the studied material was obtained by following the dynamic material model. Microstructural characterization studies conducted on the compressed composite samples using optical and scanning electron microscopy, revealed dynamic recrystallization, debonding of Ti Particles, particle breakage, and flow localization. The observations were performed in order to describe the behaviour of the material under hot forming operation in terms of material damage and micro structural modification [33]. A new bimetal magnesium/aluminium (Mg/Al) macrocomposite containing mm-scale Al core

reinforcement was fabricated via casting and hot coextrusion. Characterization revealed fairly uniform Al volume fraction along the extruded rod length attributable to mechanical interlocking between Mg shell and Al core. Major defects were absent and Mg–Al interfacial integrity was good. Thermal stability of the macrocomposite was marginally improved when compared to pure Mg. Results revealed that the presence of the Al core leads to a decrease in strength of Mg, but an improvement in stiffness as well as significant increase in failure strain (144%) and work of fracture (73%) of Mg. An attempt is made in the present study to investigate the effect of presence of mm-scale Al core on the microstructure and mechanical properties of the bimetal Mg/Al macrocomposite [34]. Yadav and Bauri [4,5] fabricated the Ni particle embedded aluminium matrix composite by friction stir processing (FSP). The FSP resulted uniform dispersion of nickel particles in the aluminium matrix with excellent interfacial bonding and grain refinement of the matrix. The composite exhibited threefold increase in the 0.2% proof stress with retaining an appreciable amount of ductility. Wu et al. [35] studied the effect of Mo addition on the microstructure and wear resistance of in-situ TiC/Al composite using a casting route assisted by self-propagating high-temperature synthesis. The experimental results exhibited that the Mo improves the wettability between TiC and aluminium melt due to the formation of a Mo-rich shell around the TiC particles. As compared to the non-Mo added composite, the addition of 1.0 wt% Mo developed finer matrix structure, significant refinement and uniform distribution of TiC particles in the matrix. It is also reported that both wear and tensile properties of TiC/Al composite were improved with 1.0 wt % Mo addition. However, the further increase of Mo content deteriorates the properties owing to the formation of fragile Al_5Mo phase.

2.3.2. MMCs reinforced with nano ceramic particles:

Wang et al. fabricated in situ 100-200 nm Al_2O_3 particles reinforced Al composites by direct melt reaction process. They observed the in situ generated Al_2O_3 particle shaving various irregular shapes disperse uniformly in the matrix with the clean interface between particle and matrix. They observed high density of dislocations generated extensive fine subgrains around the Al_2O_3 particles and concluded that the composites are comprehensively strengthened not only by Al_2O_3 particles, but also by the high density dislocations and fine subgrains [36]. Mazahery and Ostadshabani incorporated alumina nanoparticles into the A356 aluminium alloy by a mechanical stirrer and cylindrical specimens were cast. A uniform distribution of reinforcement, grain refinement of aluminium matrix, and presence of the minimal porosity was observed by microstructural characterization of the composite samples. Characterization of mechanical properties revealed that the presence of nanoparticles significantly increased compressive and tensile flow stress at both casting temperatures. It was revealed that the presence of nano-Al_2O_3 reinforcement led to significant improvement in 0.2% yield strength and ultimate tensile stress while the ductility of the aluminium matrix is retained. Fractography examination showed relatively ductile fracture in tensile-fractured samples [37]. Su et al. [5] fabricated the nano Al_2O_3/2024 composites by solid–liquid mixed casting combined with ultrasonic treatment. The composite exhibited fine grain, reasonable Al_2O_3 nanoparticles distribution in the matrix, and low porosity. Solid–liquid mixed casting technique was effective in inhibiting the agglomeration of nanoparticles in the matrix. The application of ultrasonic vibration on the composite melt during the solidification not only refined the grain microstructure of the matrix, but also improved the distribution of nano-sized reinforcement. Compared with the matrix, the ultimate tensile strength and yield strength of 1 wt% nano-Al_2O_3/2024 composite were enhanced by 37% and

81%, respectively. The better tensile properties were attributed to the uniform distribution of reinforcement and grain refinement of aluminium matrix [5].

2.3.3. MMCs reinforced with both micro and nano ceramic particles:

The effects of the addition of Al_2O_3 particle reinforcements of different sizes (5 vol% each of micro and nano) on the microstructure, physical and mechanical properties of magnesium based composite was studied by Wong et al [38]. Powder metallurgy involving microwave assisted rapid sintering technique was adopted as the synthesis route. Minimal porosity was observed in all the samples. The mechanical properties like hardness, elastic modulus,0.2% yield strength, ultimate tensile strength showed an noticeable increase on addition of micron and nano-sized particle reinforcements in magnesium matrix, whereas the ductility somewhat decreased as compared to pure magnesium. When nano-sized alumina particles were used from 0.5 to 0.75vol%, there was an increase in elastic modulus and ductility, while no subsequent changes in other mechanical properties. But, as the vol fraction reached 1%, an improvement was observed in almost all properties. Sajjadi et al. [39] used compocasting to fabricate aluminum–matrix composite reinforced with micro and nano-alumina particles. The microstructure of the composite revealed that application of compocasting process led to a transformation of a dendritic to a nondendritic structure of the matrix alloy. The SEM micrographs revealed that Al_2O_3 nano particles were surrounded by silicon eutectic and inclined to move toward inter-dendritic regions. They were dispersed uniformly in the matrix when 1, 2 and 3 wt.% nano Al_2O_3 or 3 and 5 wt.% micro Al_2O_3 was added, while, further increase in Al_2O_3 (4 wt.% nano Al_2O_3 and 7.5 wt.% micro Al_2O_3) led to agglomeration. The density measurements showed that the amount of porosity in the composites increased with increasing weight fraction and speed of stirring and decreasing particle size. The hardness

results indicated that the hardness of the composites increased with decreasing size and increasing weight fraction of particles [39].

2.3.4. MMCs reinforced with both metallic and ceramics particles:

In one of the research study of Q.B. Nguyen and M. Gupta [40], different amounts of Ca (1 wt. %, 2 wt. % and 3 wt. %) were incorporated into a AZ31B/nano-Al_2O_3 magnesium alloy composite using the disintegrated melt deposition (DMD) technique followed by hot extrusion. The samples were characterized in terms of physical, microstructural and mechanical properties. Microstructural characterization studies revealed that with increasing Ca addition, the matrix grain size and the presence of $Mg_{17}Al_{12}$ phase reduced. On the contrary, it was observed that the presence of Al_2Ca phase increased. Furthermore, the presence of Ca significantly assisted in improving 0.2% yield strength (YS) and ultimate tensile strength (UTS) while failure strain (FS) was reduced. An attempt is made to correlate the effect of increasing amount of Ca on the microstructure and mechanical properties of AZ31B/nano-Al_2O_3 composite [40]. Again, Q.B. Nguyen and M. Gupta synthesized a hybrid AZ31B alloy based composite by using a solidification processing route [41]. But in this case, along with the nano- alumina particles, copper was added as a metallic reinforcement. The involvement of the duo led to an improvement in microstructural characteristics (reduced interparticle spacing), dimensional stability, hardness and overall tensile response of AZ31B. In case of AZ31B–Cu–Al_2O_3 samples there was mixed-type fracture with limited presence of microcrack whereas, AZ31B–Cu samples presented significant presence of microcracks and the breakage of Cu particles. It can be concluded that these type of alloy-composite (hybrid; metallic+ceramic reinforcements) has the ability to excel in diverse engineering applications when compared to AZ31B or AZ31B–Al_2O_3 nanocomposites. Similar type of behaviour was observed in a nano-composites (AZ31B–3.3Al_2O_3–Cu) based on magnesium

alloy AZ31B ,developed using DMD technique[42]. Here, in addition to all of the properties mentioned in the above two cases, the compressive strength also increase with increase in amount of copper addition along with alumina while reducing ductility [42].

Chapter 3

Materials and experimental procedure

3.1. Specimen fabrication

3.1.1. Raw materials:

For this research we had chosen commercially available pure aluminum of purity >98% and particle size 50μm as our matrix. Titanium of microns and alumina (both in nano and microns) were used as the reinforcements.

3.1.2. Blending:

To begin with the powder metallurgy method, we first blended the powders in right proportion. The blending process was carried out in Abrasion Tester for 2 revolutions. Titanium and alumina both were added in same 8 vol% with matrix pure aluminum differently to get five distinct combinations.

Table 3.1: Various combinations of the Ti and Al_2O_3 particles in the composites and their corresponding abbreviated nomenclature

Materials used	Abbreviated nomenclature
Al+Macro Ti particles	Al+Ti
Al+Macro Al_2O_3 particles	Al+MA
Al+Nano Al_2O_3 particles	Al+NA
Al+Ti+Macro Al_2O_3 particles	Al+Ti+MA
Al+Ti+Nano Al_2O_3 particles	Al+Ti+NA

3.1.3. Compaction:

Following the blending of the powders, the green compact of 15mm diameter was produced in an electrically operated uni-axial cold compaction machine at an applied pressure of

600MPa. The aspect ratio (l/d) of 15mm dia pellets was maintained at 0.8 as per ASTM- E09 standards. For this purpose a stainless steel die of internal diameter of 15mm was used. The wall of the die was properly lubricated by zinc stearate. After every compaction, the system was kept in hold for 2min to reduce the anti-effects of the back-pressure produced.

3.1.4. Sintering:

The sintering of the green compacts was carried out in a tubular furnace under argon atmosphere. First of all the tube was evacuated to a vacuum level of 10^{-5}bar and the samples were placed on a crucible inside the chamber. Then Ar gas was supplied at 200ml/min so that no oxidation takes place during sintering, since Aluminium is very much prone to get oxidized. Four samples of each of the combinations mentioned in table1 were sintered at 600°C for 120min. On completion of sintering, all samples were left to cool down to room temperature inside the furnace itself before exposing it to outside atmosphere.

3.2. Specimen characterization

3.2.1. XRD analysis:

In order to study the phases present in the specimen, X-ray diffraction (PANalytical model: DY-1656) was done using CuKα (λ=1.5418A°) radiation. The scanning range used for the diffraction was 10°- 90° with a step size of 2°/min.

3.2.2. Scanning Electron Microscopy (SEM) observation:

The microstructure was characterized by scanning electron microscope (JEOL 6480 LV). We used Keller's reagent (1.5%HCl, 1%HF, 2.5%HNO_3 and rest distilled water) for etching the

specimen. 20kV was maintained as the accelerating voltage for all of the micrographs. Here we concentrated on how the particles were distributed, interface bonding between reinforcement particle and matrix, grain size, etc. The samples after wear and corrosion tests were also visualized under SEM.

3.2.3. Density measurement:

Theoretical density was estimated on the basis of rule of mixtures.

$$\rho_{composite} = (\rho_{Al} \times \text{vol\% of Al}) + (\rho_{reinforcement} \times \text{vol\% of reinforcement})$$

where, the second term 'reinforcement' on the R.H.S of the above equation denotes to either of the earlier mentioned combinations (table 1). The sintered density was measured by Archimedes Method. The weight of the pellets were first measured in air and then in distilled water. Contech CB series analytical balance with a density measurement kit package from Contech was used for the density measurements.

3.2.4. Hardness measurement:

The microhardness was measured on the polished surface of the specimen by the help of Vickers hardness tester (Leco Microhardness Tester LM248AT). The indentation was made by a load of 100gf with a dwell time of 10secs. For each of the sample, eight readings were taken considering the average of their values as the hardness of the same.

3.2.5. Wear tests:

Wear tests were carried out in dry sliding condition in accordance with the ASTM G-99 standard using a pin-on-disc wear and friction monitor model no. DUCOM;TR-20-M100. The machine consists of an EN32 steel disc having a hardness value of HRC 58 and diameter of 100 mm. The cylindrical specimens of 6 mm diameter and 12 mm height were machined.

Wear tests were carried out at the normal load of 30 N. All the tests were carried out at a fixed distance of 100 mm from the centre of the disc at 300 rpm, corresponding to a linear velocity of 1.57 m/s for a constant sliding distance of 1.0 km. During the wear test, the height loss of the sample was continuously monitored and it was converted to volume loss (in mm^3) by multiplying it with the cross-sectional area. The wear rate (in mm^3/m) was obtained by dividing the volume loss with the sliding distance (in m). Before and after each test, both the disc and the specimens were cleaned thoroughly with acetone and then dried in order to avoid contamination. Each test was carried out at least twice in order to check the reproducibility and average value of the tests was taken to determine the wear rate.

3.2.6. Compression tests:

The compressive strength of the composite was measured in a universal testing machine (Instron- SATEC series servo-hydraulic machine) at a crosshead speed of 0.5mm/min. The nominal diameter and height of all samples tested were 15 and 12 mm, respectively as per the ASTM E9-89 standard.

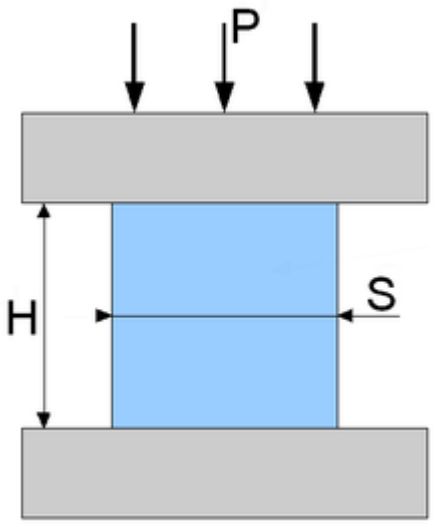

Fig 3.1: Load application during uni-axial compression test.

3.2.7. Corrosion tests:

Corrosion tests were performed on all the specimens after slightly grinding the surfaces with silicon carbide paper (2500 grit, deionized water cooling). Finally, all the specimens were cleaned in alcohol prior to corrosion test. Electrochemical corrosions tests were carried out in aqueous 3.5 wt.% NaCl solution saturated with atmospheric oxygen and adjusted to neutral pH using NaOH with an exposed area of 0.5 cm^2 using a Gill AC potentiostat/galvanostat. The corrosion cell (333 ml) with a typical three electrode set-up, with the specimen as the working electrode, a saturated Ag/AgCl electrode as reference electrode and a platinum mesh as counter electrode was used. The electrolyte temperature was controlled at 22± 0.5°C and the electrolyte was stirred during the experiments. One experiment lasted for about 19 hours and consisted of three subsequent tests as follows.

i. Recording of the free corrosion potential for 5 minutes.

ii. Potentiodynamic polarization scans starting from −150 mV relative to the free corrosion potential with a scan rate of 0.2 mV/s. The test was terminated when a corrosion current density of 0.1 mA/cm^2 was exceeded to minimize the damage on the specimen surface before the next sequence started. This test lasted for about 30 minutes. From the cathodic branch of the polarization curve the corrosion rate was determined using the Tafel slope.

iii. Subsequently, Electrochemical Impedance Spectroscopy (EIS) measurements at free corrosion potential were carried out using a Gill AC over the frequency range from 10 kHz to 0.01 Hz. The amplitude of the sinusoidal signals was 10 mV. The EIS scans were conducted at the interval of 3, 6, 9, 12, 15 and 18 hours of immersion. The charge transfer resistance was calculated from the intersections of the circle with the real axis (0° phase shifts) giving the solution resistance and the sum of the

solution and the charge transfer resistance respectively (assuming a simple Randles circuit model).

After the corrosion tests, the specimens were ultrasonically cleaned and observed under microscope.

Chapter 4

Results and discussion

4.1. Synthesis

Pure Al and its composites were successfully synthesized using powder metallurgy technique coupled with conventional sintering technique. The results of the characterization studies performed on the materials clearly indicate the feasibility of using conventional sintering to develop Al composites.

4.2. Density and porosity

Table 4.1 shows the density and porosity measurement values for all the Al-based composites. It can be seen that the density values increased with the addition of both metallic and ceramic particles as compared to that of pure Al (density 2.7 g/cc). The increase in density for the Al+Ti composite is more as compared to that of the composites reinforced with macro and nano-sized Al_2O_3 particles. There is a difference between the experimental density and the theoretical density values. This indicates the porosity present in all the composites is significant, which is the characteristics of the materials processed via powder metallurgy technique with conventional sintering. It is also true that in the present investigation no secondary processing (like extrusion) was carried out, which generally reduce the existing porosity to some extent. It is also observed that the porosity level is reduced in case of the composite reinforced with macro-sized Al_2O_3 as compared to the composite reinforced with nano-sized Al_2O_3. The similar trend in porosity results i.e., decrease in porosity per cent with increase in particle size was also observed earlier by Sajjadi et al. in the A356 alloy composites reinforced with macro and nanoAl_2O_3 and processed by compocasting [39]. The results also exhibited an increase in the density with increase in the total content of Ti and Al_2O_3 in the Al matrix. This can be attributed to higher density of Ti (4.507 g/cm^3) and Al_2O_3 (3.95 g/cm^3) particles as compared to that of pure Al (2.7 g/cm^3) matrix.

Table 4.1: Results of density and porosity measurements for the Al-based composites

S. No.	Material	Experimental density (g/cm^3)	Theoretical density (g/cm^3)	Porosity (%)
1	Al+Ti	2.7783	2.8445	2.33
2	Al+NA	2.7120	2.8000	3.14
3	Al+MA	2.7416	2.8000	2.08
4	Al+Ti+NA	2.8643	2.9500	2.90
5	Al+Ti+MA	2.8758	2.9500	2.52

4.3. XRD analysis

Fig.4.1 shows the X-ray diffraction patterns for all the fabricated Al-based composites. The experimental data obtained were compared with that of the standard powder diffraction results for Al, Ti, Al_2O_3 and Al_3Ti intermetallic phases. It is evident that all the composites exhibited peaks corresponding to pure Al along with the peaks corresponding to pure Ti in case of Al+Ti; Al_2O_3 in case of Al+NA and Al+MA; Ti and Al_2O_3 in case of Al+Ti+NA and Al+Ti+MA composites. Apart from these phases, few peaks corresponding to the intermetallic phases Al_3Ti are also present in the Al+Ti, Al+Ti+NA and Al+Ti+MA composites, which are produced by the reactions of Al with Ti. The studies conducted so far have shown that the addition of Ti in the Al leads to a reaction between Ti and Al to form Al_3Ti through peritectic reaction. The interaction between Ti and Al results in either a solid solution of Ti in Al (with a very limited solid solubility) or the formation of Al_3Ti through peritectic reaction [43]. The microstructures of Al–Ti synthesized by using conventional casting with slow cooling rate, spray atomization and deposition with reasonably high cooling rates revealed the as-expected existence of Al_3Ti intermetallic phase. Thus, the intermetallic phase Al_3Ti, which is present in Al-Ti system, is not beneficial for the

development of composites. The formation of the intermetallic phase Al_3Ti in the Al-Ti system has also been reported by several researchers.

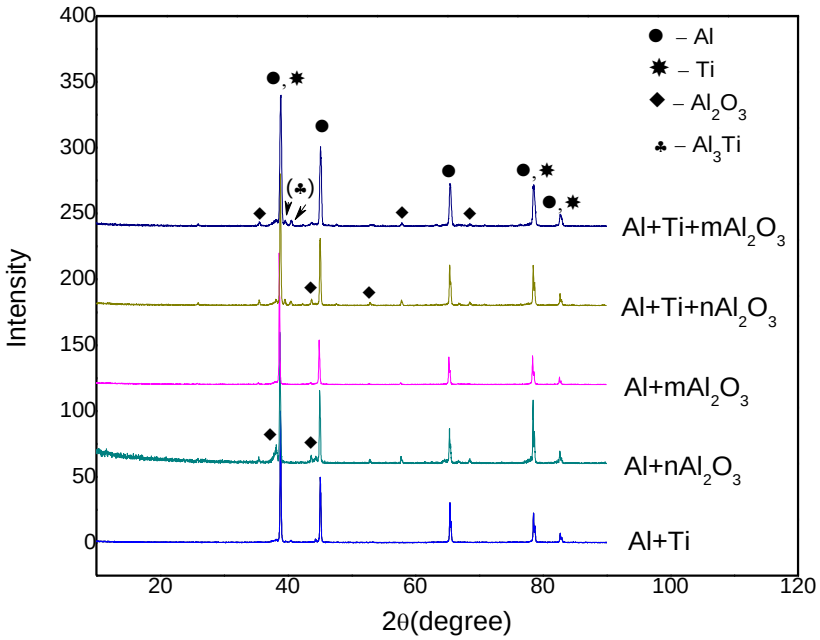

Fig 4.1: X-ray diffraction patterns obtained from all the Al-based composites

4.4. Microstructure

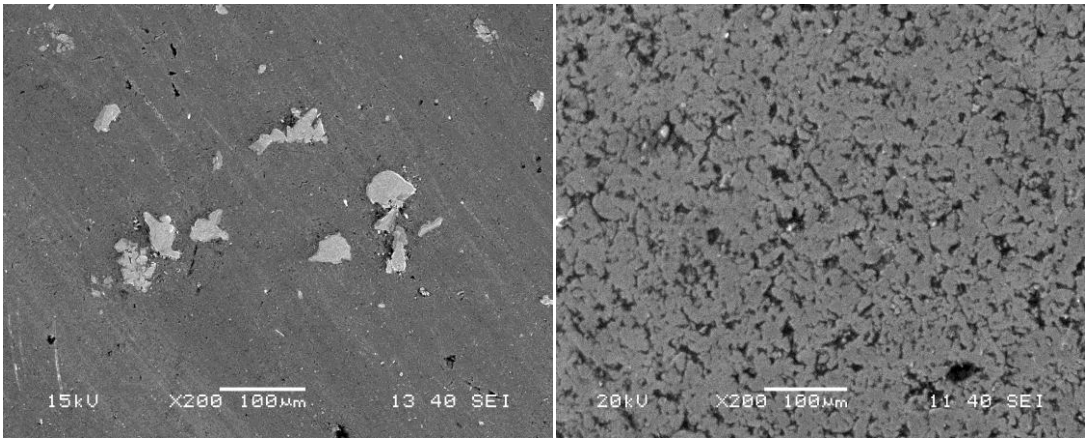

(a) (b)

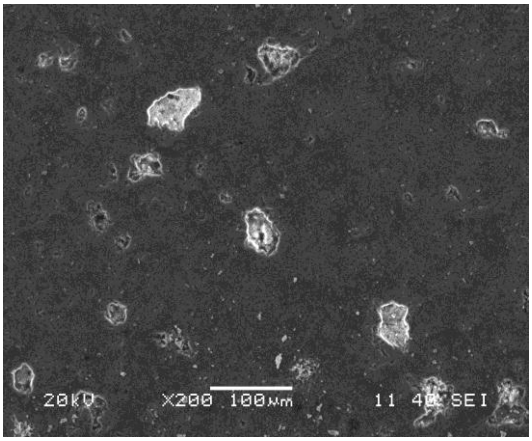

(c)

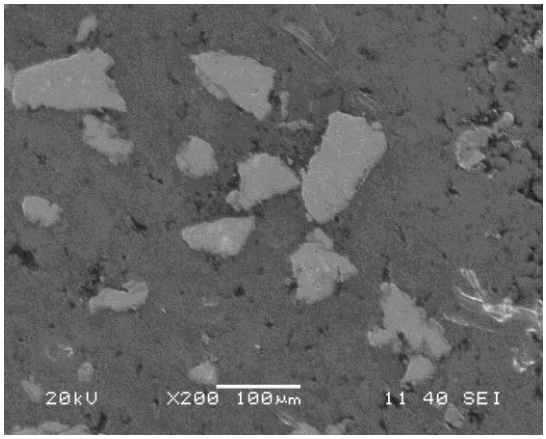

(d)

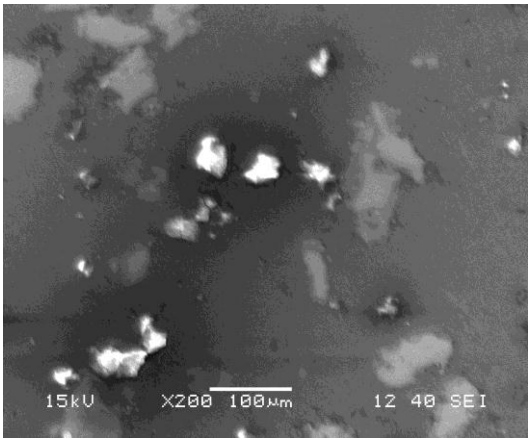

(e)

Fig 4.2: Representative as sintered SEM micrographs for all the Al-based composites corresponding to: (a) Al+Ti; (b) Al+NA; (c) Al+MA; (d) Al+Ti+NA and (e) Al+Ti+MA.

Fig. 4.2 (a-b) shows the SEM micrographs obtained from the as-received Ti and Al_2O_3 powders. It is evident that there is no significant difference in grain size and appearance of the Ti powder and the same is true for the Al_2O_3 power as well. Fig.4.2 (a-e) shows the representative microstructures for all the composites. The micrographs revealed the presence of porosity in all the composites and the extent of porosity present is more in case of the composites reinforced with nano-sized Al_2O_3 (Fig. 4.2 (b and d)) alone. This is also supported by the experimental porosity results obtained using density measurement as shown in Table 4.1. It is evident from Fig. 4.2 (a,d,e) that the metallic Ti particles were uniformly distributed in the Al+Ti, Al+Ti+NA and Al+Ti+MA composites. However, the intermetallic

1phase (Al_3Ti) formed owing to the metallic addition was not observed in the representative micrographs (Fig. 4.2 (a,d,e)) taken at low magnification. There is no nano-Al_2O_3 particles agglomeration in the composites, as observed in the BSE image (Fig. 4.3).Therefore, the clustering of the reinforcing particles in general is negligible in all the composites employed. The interfacial integrity was assessed in terms of interfacial debonding and the presence of microvoids at the interface. The micrographs of the composites exhibited good interfacial integrity between the matrix and the reinforcements. The absence of debonding or discontinuity at the interface indicated superior sintering. The micrographs also revealed almost no interfacial reaction (at the interface of Ti/Al-matrix and Al_2O_3/Al matrix) for all the composites. The microstructural analysis of Al+NA composite exhibited the significant grain refinement obtained following the addition of nano-sized Al_2O_3 particles. The decrease in grain size following the additions of micron-sized Ti and Al_2O_3 is relatively lower as compared to that obtained with the addition of nano-sized Al_2O_3. The combined addition of micron-sized Ti and nano-sized Al_2O_3 leads to the reduction in grain size in case of the composite Al+Ti+NA as well. The reduction in grain size observed is mainly due to the nano-sized Al_2O_3 particles acting as sites for grain nucleation during solid-state processing. Further, the presence of relatively harder Al_2O_3 particles inhibits grain growth, thus resulting in fine grain size. Similarly, the presence of nano-sized Al_2O_3 and Ti in the Al+Ti+NA composite restricts the grain growth due to its ability to nucleate Al grains and resulting in a significant reduction in average grain size.

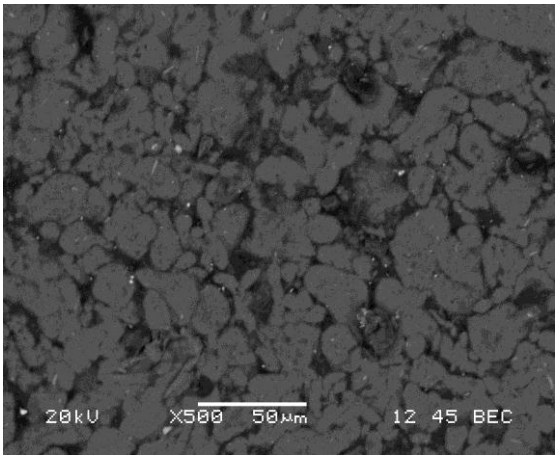

Fig. 4.3: SEM micrograph (in BSE mode) of the composite Al+NA showing minimum agglomeration of nano-Al_2O_3 particles

4.5. Microhardness

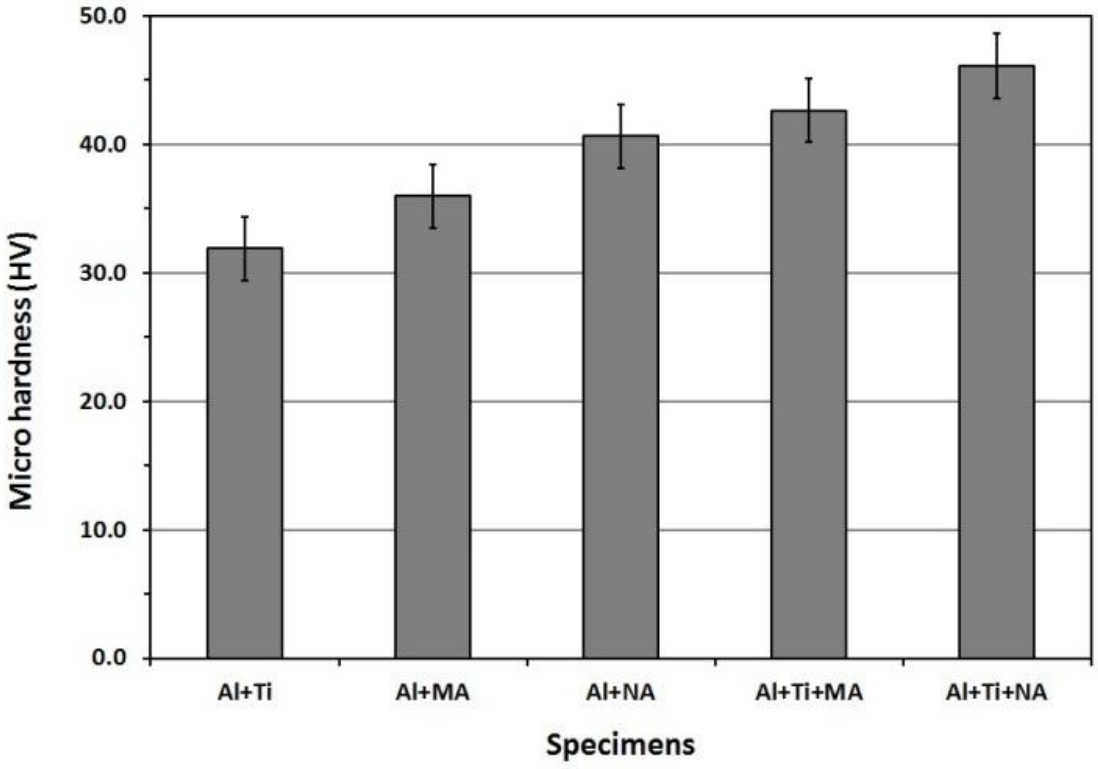

Fig 4.4: Variation of the average microhardness values for all the Al-based composites

The variation of the average microhardness values for all the composites is shown in Fig. 4.4 . It is evident from the figure that the composites reinforced with the ceramic particles (micro or nano) alone exhibited higher hardness values as compared to the composite reinforced with metallic particles alone. In addition, the composites reinforced with the nano-sized Al_2O_3 particles alone exhibited higher hardness value as compared to the composite reinforced with the macro-sized Al_2O_3 particles alone. Further a relatively higher hardness values were obtained only when the ceramic particles were added in combination with the metallic particles (i.e., hybrid composites) as compared to the composites reinforced with the individual particles. Again the Al+Ti+NA hybrid composite exhibited superior hardness value as compared to that of the hybrid composite Al+Ti+MA. The increase in hardness of the composites reinforced with the Ti metallic particles and nano-sized Al_2O_3 can be attributed primarily to (i) an increase in the presence of harder intermetallic phases and nano-Al_2O_3 ceramic particles [44] and (iii) the enhanced grain refinement observed on the Al+Ti+NA composite. This is consistent with earlier observations made on pure Mg–Cu, AZ91–Cu, and AZ31B–Al_2O_3 [45-47].

4.6. Compression behaviour

The stress values withstand by all the composites specimens at their 50% reduction of height are reported here.

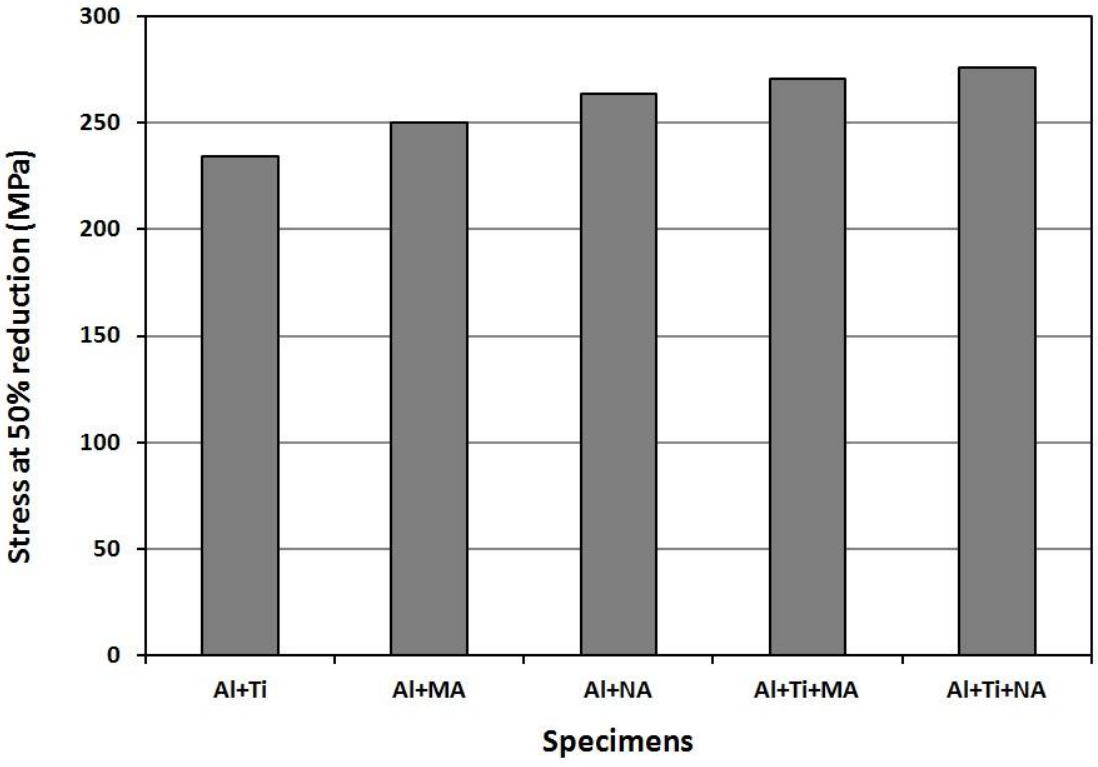

Fig. 4.5: Comparison of the stress values withstand at 50% reduction of the composites specimens

The stress values obtained here (Fig 4.5) is not the ultimate compressive stress but the stress at which the material is reduced to 50% of its initial height. From the plot we can observe that the composites reinforced with the ceramic particles (micro or nano) alone sustained higher stress values as compared to the composite reinforced with metallic particles alone. In addition, the composites reinforced with the nano-sized Al_2O_3 particles alone sustained higher stress value as compared to the composite reinforced with the macro-sized Al_2O_3 particles alone. Further the hybrid composites sustained higher stress values as compared to the composites reinforced with the individual particles. Again the Al+Ti+NA hybrid composite sustained higher stress value as compared to that of the hybrid composite Al+Ti+MA. The increase in strength of the composites Al+NA and Al+Ti+NA might be owing to Orowan strengthening and grain refinement observed on the nano composites.

4.7. Dry sliding wear behaviour

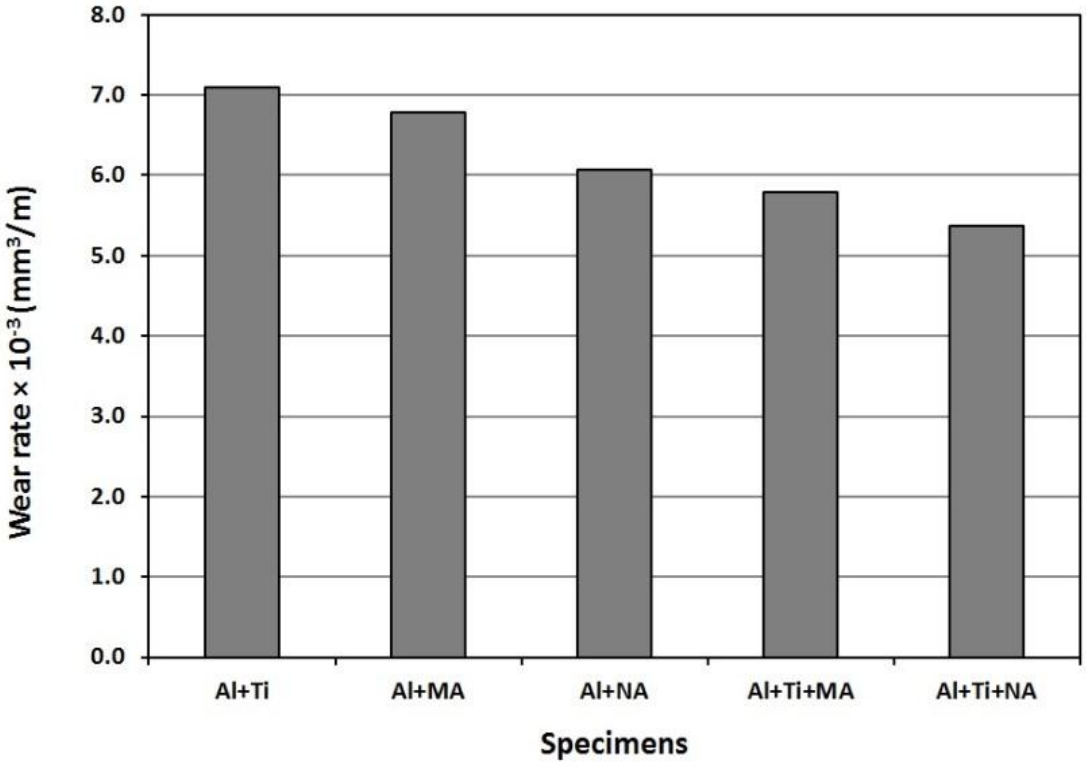

Fig 4.6: Variation of the volumetric wear rate for the Al-based composites tested using 30 N load and sliding speed of 1.5 m/s.

4.7.1. Wear rate

The wear rate in terms of mm^3/m at a speed of 1.5 m/s for the all the composites is shown in Fig. 4.6 . It is evident from the figure that the wear rate varies almost in inverse proportion with the hardness of all the composites tested, as generally expected. The wear rate of the composite Al+Ti is the highest among the composites tested at the same load. The composite Al+NA exhibits 10% better wear resistance than the composite Al+MA and the wear rates of both the composites are lower by 14% and 4%, respectively than that of the composite Al+Ti. The hybrid composites which has got higher total volume fraction of reinforcement than the rest of the composites exhibited a further decrease in wear rate at the load value employed

and it is better than all other composites tested. The Al+Ti+NA hybrid composite exhibit a 7% lower wear rate than the hybrid composite Al+Ti+MA. The lowest wear rate is exhibited by the hybrid composite Al+Ti+NA and it is 24% better than the Al+Ti composite. Thus, the wear resistance increases with the combine addition of metallic and ceramic particles in the Al matrix at the same load.

4.7.2. Observation of the worn surfaces

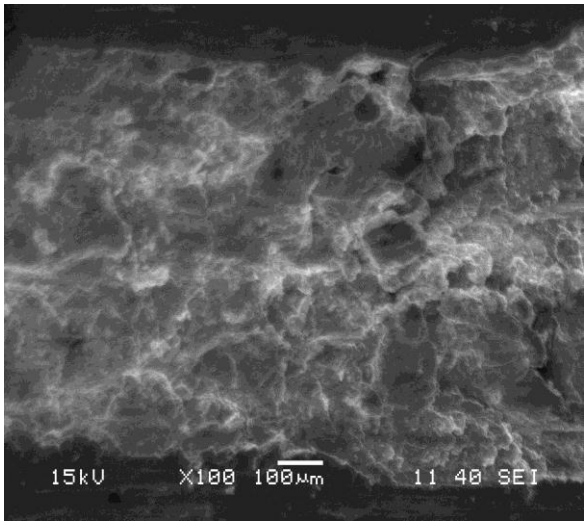

(a)

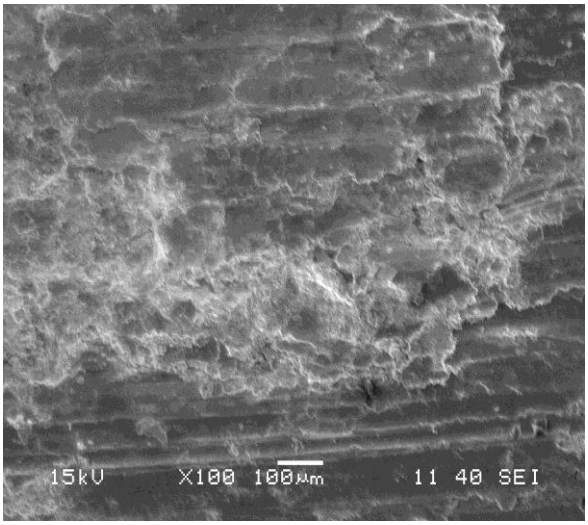

(b)

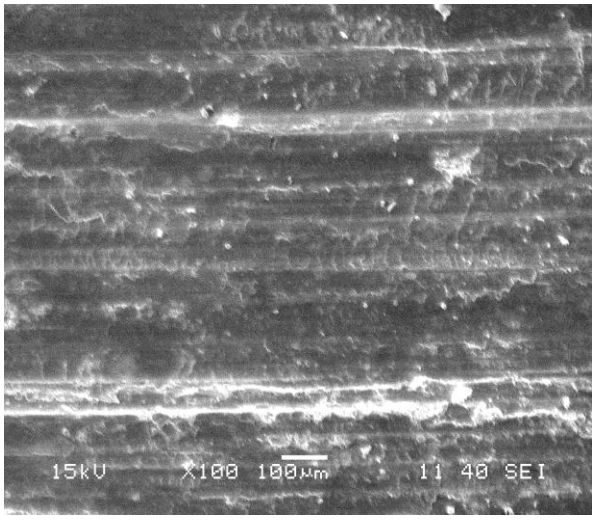

(b)

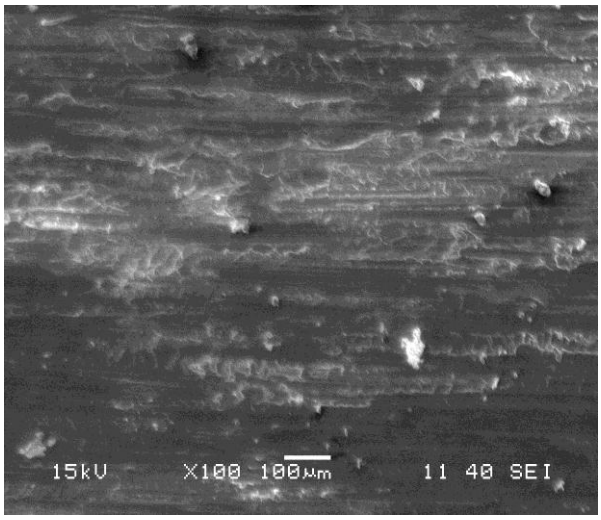

(d)

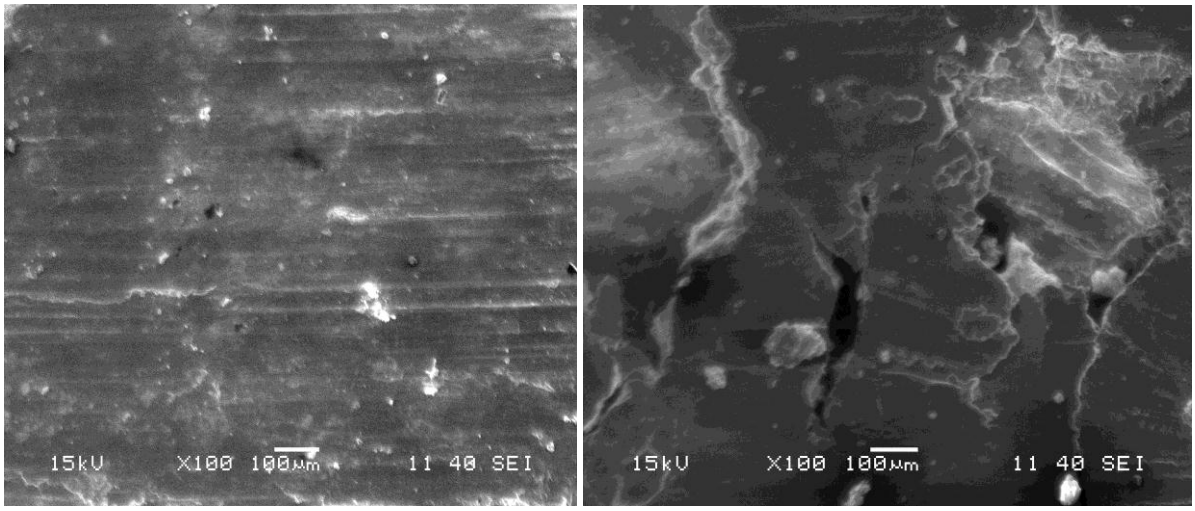

(e) (f)

Fig 4.7: SEM micrographs of the worn surfaces corresponding to the (a) Al+Ti;(b) Al+MA; (c) Al+NA; (d) Al+Ti+MA; (e) Al+Ti+NA and (f) Magnified view of (a)

Fig.4.7 (a-e) shows the micrographs of the worn surfaces of all the composites tested at 30 N load at a sliding speed of 1.5 m/s. Fig. 4.7 (a) shows the worn surface of the Al+Ti composite and the magnified view of the same is shown in Fig. 4.7 (f).It is evident from the figure that the surface is severely damaged and the extensive materials is removed from the surface by delamination, which is a dominant wear mechanism reported for the composites during dry sliding wear test. The micrographs of the worn surfaces of the rest (i.e., Al+MA, Al+NA, Al+Ti+MA and Al+Ti+NA) composites reveal that numerous long continuous and deep grooves had formed on the wear surfaces. These parallel grooves are the proof of micro ploughing and micro cutting and these indicates that the prominent wear mechanism in these composites is abrasion. The worn surface of the Al+MA composite exhibited the most extensive deep ploughing grooves. However, the grooves are relatively shallow and the severity of micro ploughing is progressively decreases on the worn surfaces of the Al+NA, Al+Ti+MA and Al+Ti+NA samples in that order. The severity of the micro ploughing was

the lowest on the worn surface of the Al+Ti+NA composite i.e., here the basic wear mechanism remained unchanged and only the grooves became shallow. Careful observation of the worn surfaces revealed some reattachment of wear debris on the worn surfaces and these were the embedded debris.

4.7.3. Reason for difference in wear behaviour

During sliding wear the pin surface experiences a normal applied load and a tangential friction force. The subsurface undergoes plastic deformation resulting in strain gradient within the layer adjacent to the contact surface. The magnitude of the strain gradient generally increases with increasing sliding distance and applied load [49]. The presence of strain gradient within the deformed zone under worn surface is a fundamental basis of the occurrence of delamination wear. According to the delamination theory of Suh [48], the plastic deformation and dislocation movements at the subsurface region will be periodical during wear. When the dislocation density at the subsurface is sufficiently higher, microcracks are initiated. The microcracks propagate parallel to the sliding direction and coalesce at the subsurface. Finally the coalesced cracks extend to the worn surface with continued sliding. The layer then disintegrates from the worn surface generating flake type debris causing severe wear.

The worn surfaces of all the composites (except Al+Ti) were covered with long continuous grooves parallel to the sliding direction (Fig. 4.7 (b–d)), which are indicative of abrasive wear. These grooves are mainly formed by the ploughing action of the hard asperities present on the hardened steel counter-face or by the trapped wear debris, which are produced during the sliding process in between the mating surfaces, causing wear by removing small fragments of the material or pushing material into ridges along the sides of the grooves. The

sliding wear of aluminium alloys and composites, particularly at low load, is generally characterized by the process of abrasion. Some reattachment of wear debris on the worn surfaces was also observed. During the sliding process, a part of the wear debris, which is produced due to the sliding contact of two surfaces, was lost from the system and the rest was remained in the mating surface. The debris particles were fragmented to a very fine size during the subsequent sliding. As the debris become finer, its surface energy increases. It reattaches to the worn surface due to the Van der Waals force as well as the electrostatic force [50].

The delamination wear resulted severe structural disruption and damage of the Al+Ti composite surface. It is known that when delamination wear is operative, the material removal will be extensive and therefore, the Al+Ti exhibited the highest wear rate among the composites tested. Extensive ploughing grooves were observed on the worn surface of Al+MA composite, however, the grooves were relatively shallow and the severity of micro ploughing was progressively decreased on the worn surfaces of the Al+NA, Al+Ti+MA and Al+Ti+NA samples in that order due to the higher hardness values of the composite surfaces, which is responsible for lower wear rates of these composites as compared to the Al+Ti composite. There have been few studies on the effect of type of reinforcements on wear resistance of composites. Hosking et al. [51] compared the dry sliding wear behaviour of an Al alloy reinforced either with 20% Al_2O_3 or 20% SiC particles of the same size (16 μm). They observed that the SiC particles offered better wear resistance due to the higher hardness than the Al_2O_3 particles. Thus, the Al+MA exhibited better wear resistance than the Al+Ti composite owing to the higher hardness of Al_2O_3 in the present investigation. There has been only one study on the effect of size of particle reinforcements (micro (100-200 μm) and nano (47 nm)) on the wear resistance of Al composites using a three pin-on-disk apparatus under

dry sliding conditions at a sliding velocity of 1.58 m/s for a normal load of 30 N by Rohatgi et al. [52]. They observed that the nano-composites exhibited the best wear performance among the composites investigated and hardness of the composites played an important role in improving the wear resistance. Thus, the Al+NA composite showed better wear resistance than the Al+MA composite owing to the higher hardness value exhibited by the former composite in the present investigation. Further, the extent of abrasive wear was lowest on the worn surface of the composite Al+Ti+NA owing to the highest hardness value obtained on it.

4.8. Electrochemical corrosion behaviour

4.8.1. Nature of the corrosion response

Fig. 4.8 shows the variation of open circuit potential for all the Al-based composites. The measurement of the open circuit potential (or free corrosion potentials) for the 5 minutes of immersion exhibited large differences among the various specimens. It is obvious that the addition of the reinforcements (except Ti particles) to the Al matrix shifts the potential to more active values, which is not good for corrosion resistance. From the start of the recording free corrosion potential the Al+Ti specimen reached stable conditions and values between −743 and −765 mV were recorded. This could be attributed to the passive film formation due to the presence of only Al and Ti in the specimen and these are known to possess excellent corrosion rate. The slopes of the two curves corresponding to Al+MA and Al+NA specimens indicated a continuous drop towards less noble potentials, indicating continuous attack on the surfaces of the two specimens. The slopes of another two curves corresponding to Al+Ti+MA and Al+Ti+NA hybrid composites became stable following an initial shallow drop, indicating the initial attack on the surfaces which was recovered later on. The open circuit potential measurements after 5 minutes of immersion exhibited the noblest potential

value for the Al+Ti specimen as compared to the other specimens and registered an average value of −755 mV, as shown in Fig. 4.9.

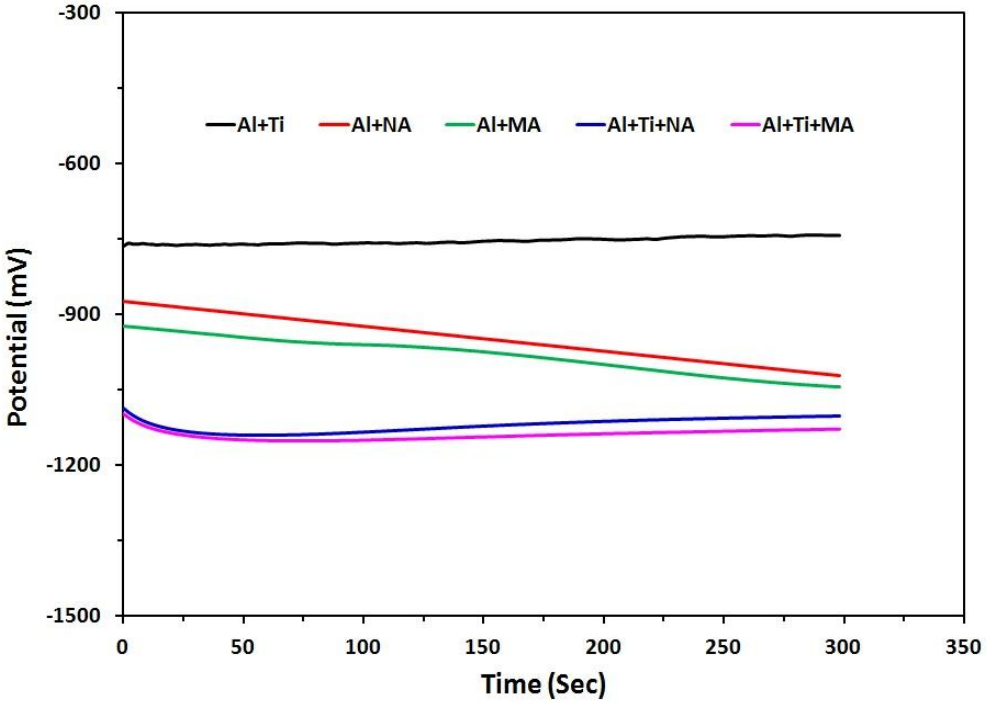

Fig 4.8: Variation of the open circuit potential for all the Al-based composites

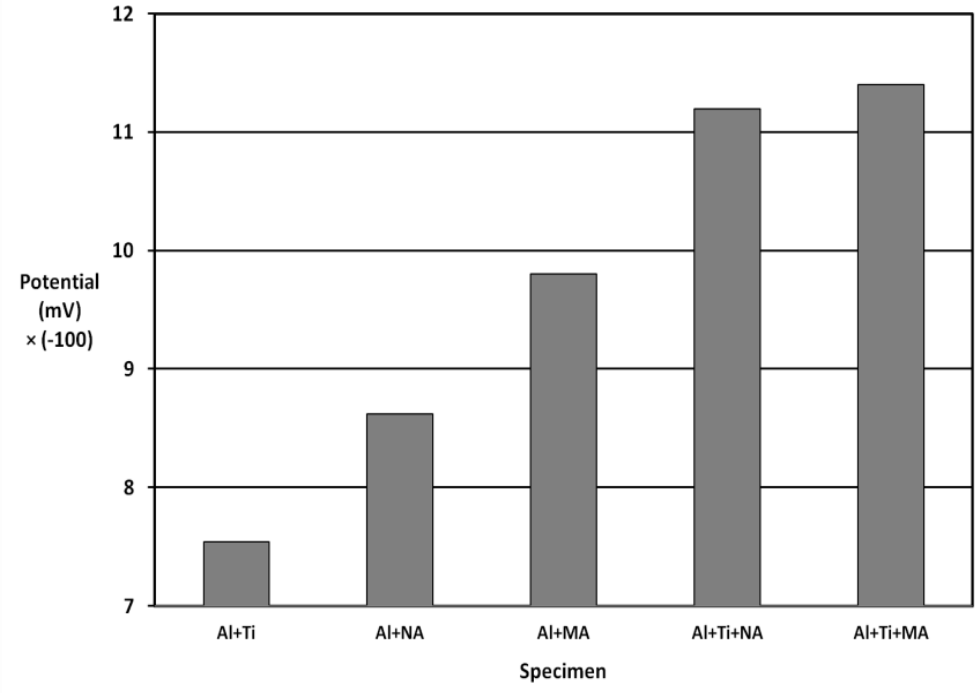

Fig. 4.9: Average values of the open circuit potential for all the Al-based composites

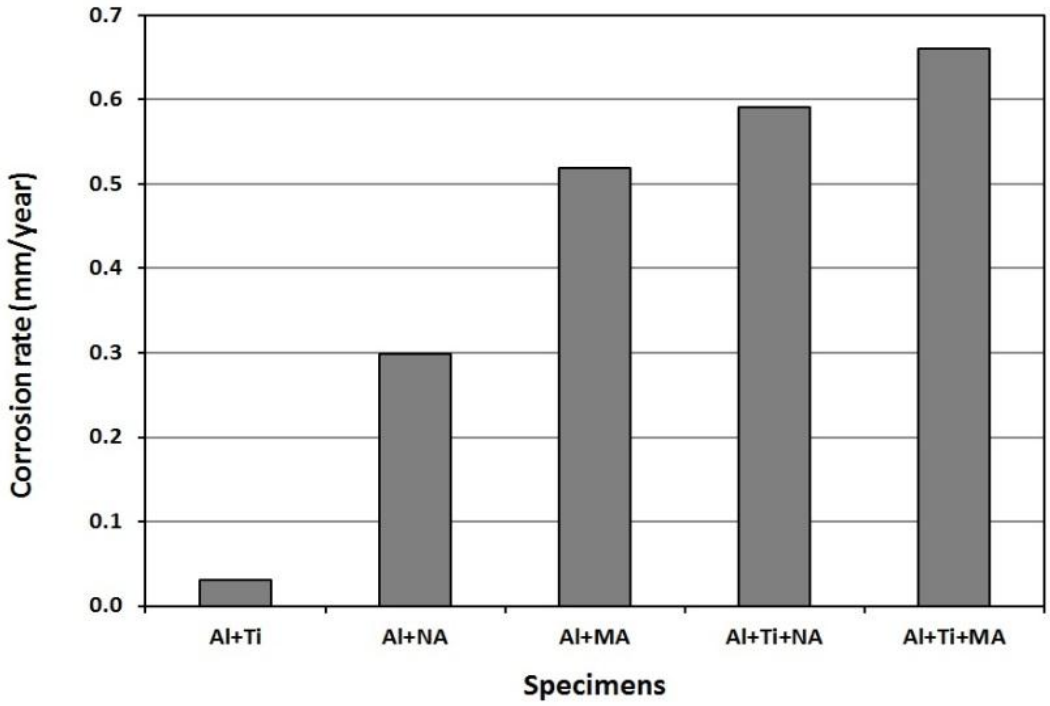

Fig. 4.10: Variation of the corrosion rates calculated from the potentiodynamic polarization plots for all the Al-based composites

Fig.4.10 shows the corrosion rates determined by potentiodynamic polarization measurements for all the Al-based composites. It is evident from the figure that the Al+Ti composite exhibited the lowest corrosion rate. The composites reinforced with the ceramic particles (micro or nano) alone exhibited higher corrosion rate as compared to the composite reinforced with metallic particles alone. In addition, the composites reinforced with the nano-sized Al_2O_3 particles alone exhibited better corrosion resistance as compared to the composite reinforced with the macro-sized Al_2O_3 particles alone. Further relatively higher corrosion rates were exhibited by the composites having combine addition of ceramic as well as metallic particles (i.e., hybrid composites) as compared to the composites reinforced with the individual particles. Again the Al+Ti+NA hybrid composite exhibited superior corrosion resistance as compared to that of the hybrid composite Al+Ti+MA.

The long term electrochemical impedance spectroscopy (EIS) was continued right after the potentiodynamic polarization measurements to follow the passivation behavior over a longer time period. The EIS measurements exhibited reasonable results. The typical Nyquist plots obtained for the all the composites after 3, 6, 9, 12, 15 and 18 hours of immersion are shown in Fig. 4.11 (a-e). It is obvious that during the longer exposure time, the differences among the composites become more transparent. The Al+Ti composite develops a continuously increasing resistance, most likely, as a result of growing passive film thickness, the other composites materials are not able to build up passive films, as shown in Fig. 4.11 (b-e). However, their resistances do not fluctuate much and remain at a very low level, indicating a clear trend in the corrosion resistance among the composites. Similar to the results of the potentiodynamic polarization, the Al+Ti composite maintained its best performance compared to the other composites. It is evident from the figure that the Al+Ti composite exhibited the lowest corrosion rate. The composites reinforced with the ceramic particles (micro or nano) alone exhibited higher corrosion rate as compared to the composite reinforced with metallic particles alone. In addition, the composites reinforced with the nano-sized Al_2O_3 particles alone exhibited better corrosion resistance as compared to the composite reinforced with the macro-sized Al_2O_3 particles alone. Further relatively higher corrosion rates were exhibited by the composites having combine addition of ceramic as well as metallic particles (i.e., hybrid composites) as compared to the composites reinforced with the individual particles. Again the Al+Ti+NA hybrid composite exhibited superior corrosion resistance as compared to that of the hybrid composite Al+Ti+MA. There is no indication of the presence of inductive part in all the curves, which suggests the absence of strong localized active dissolution of the Al in the composites. However, after longer immersion times, the composites (except Al+Ti) had the ability to repassivate again, as can be seen in Fig. 4.11 (a-f).

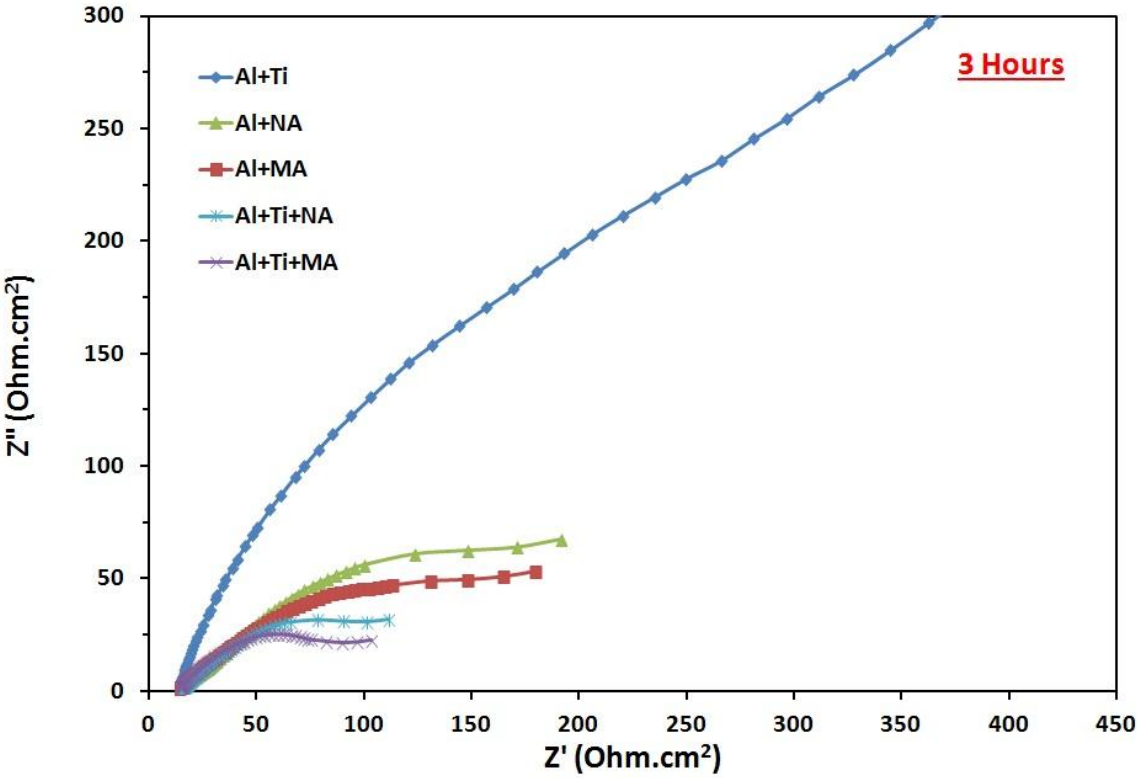
3 Hours
Al+Ti
Al+NA
Al+MA
Al+Ti+NA
Al+Ti+MA
Z'' (Ohm.cm²)
Z' (Ohm.cm²)
0
50
100
150
200
250
300
350
400
450

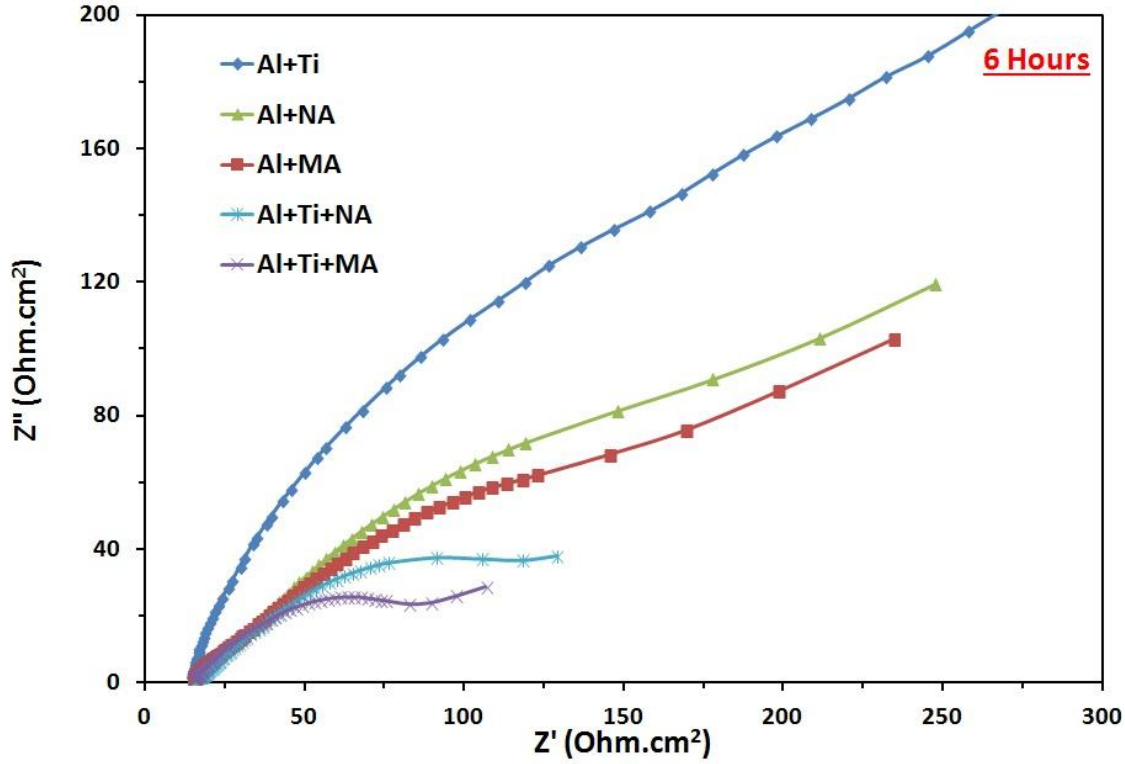
6 Hours
Al+Ti
Al+NA
Al+MA
Al+Ti+NA
Al+Ti+MA
Z'' (Ohm.cm²)
Z' (Ohm.cm²)
0
40
80
120
160
200
250
300

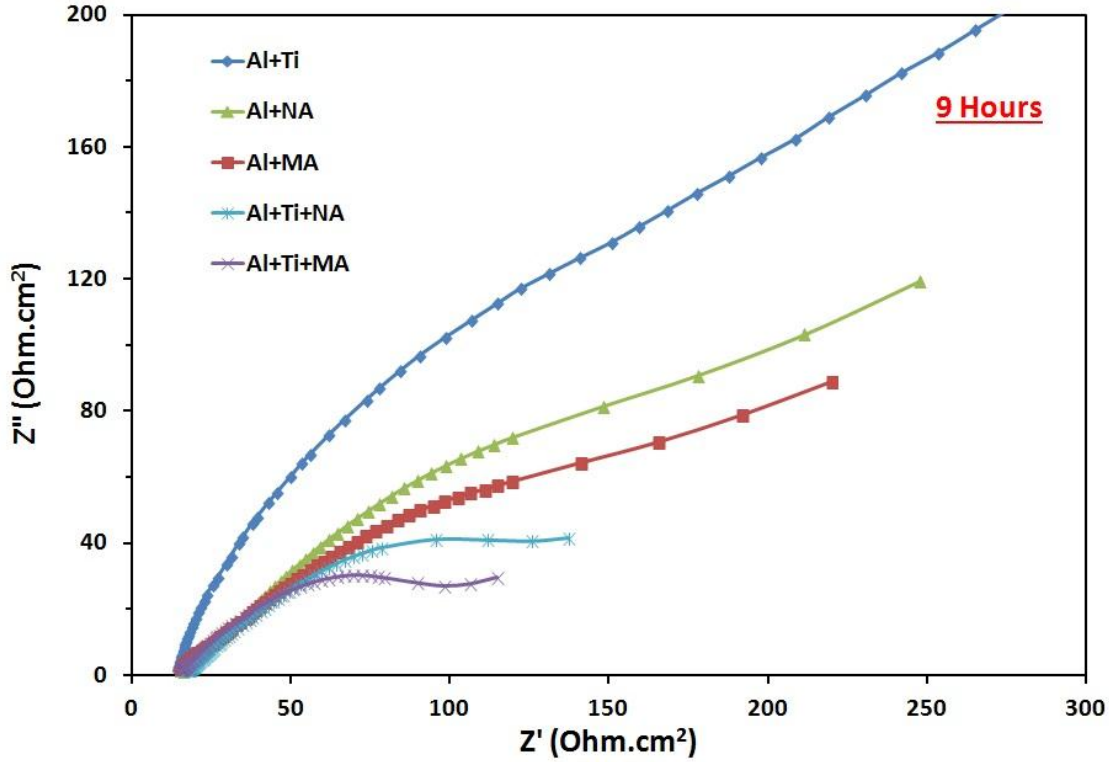
9 Hours
Al+Ti
Al+NA
Al+MA
Al+Ti+NA
Al+Ti+MA
Z'' (Ohm.cm²)
Z' (Ohm.cm²)
0
40
80
120
160
200
0
50
100
150
200
250
300

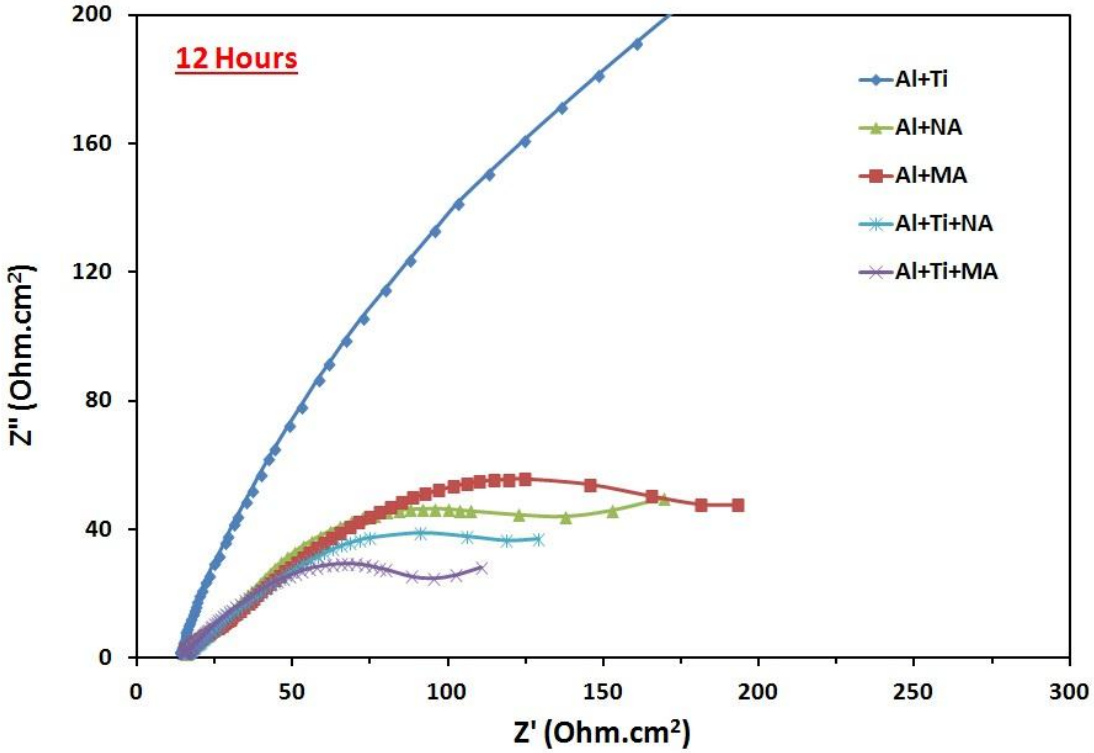
12 Hours
Al+Ti
Al+NA
Al+MA
Al+Ti+NA
Al+Ti+MA
Z'' (Ohm.cm²)
Z' (Ohm.cm²)
0
40
80
120
160
200
0
50
100
150
200
250
300

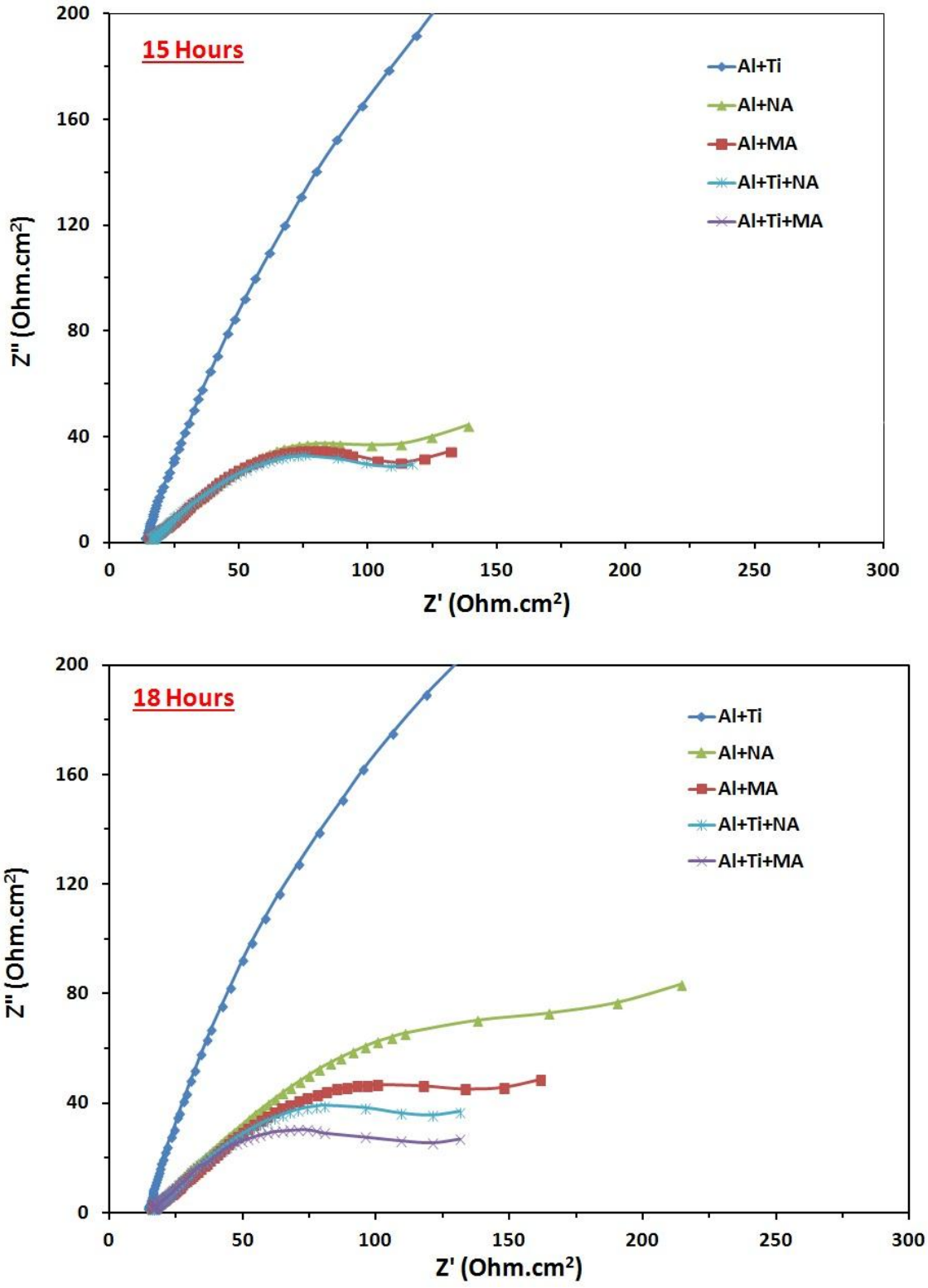

Fig. 4.11: Nyquist plots for all the composites after (a) 3 hrs (b) 6 hrs (c) 9 hrs (d) 12 hrs (e) 15 hrs and (f) 18 hrs of immersion.

4.8.2. Morphology of the corroded surfaces

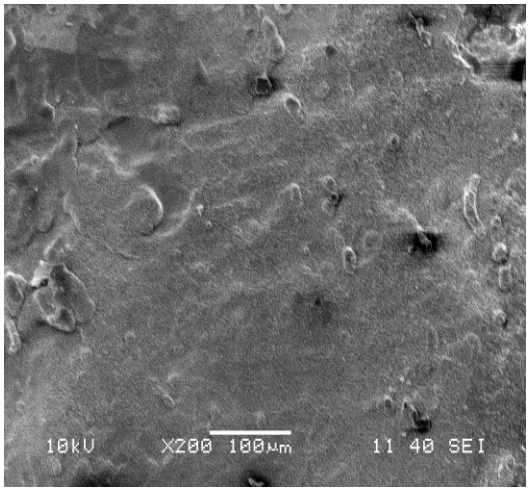

(a)

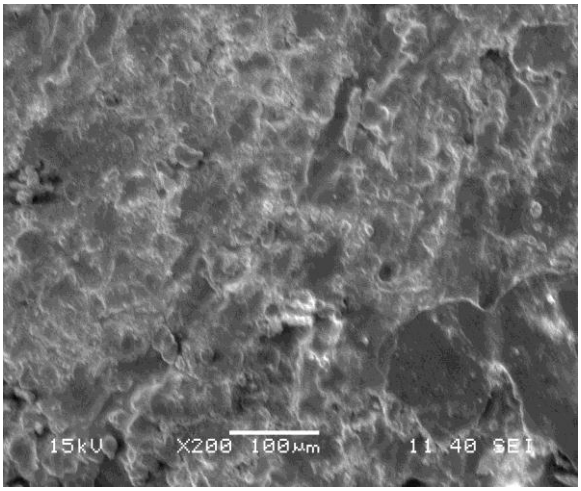

(b)

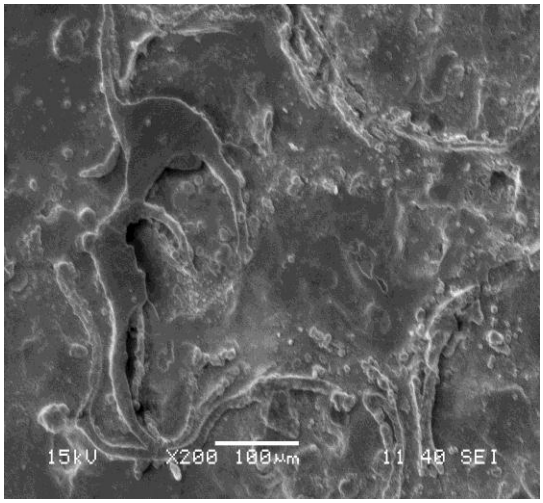

(c)

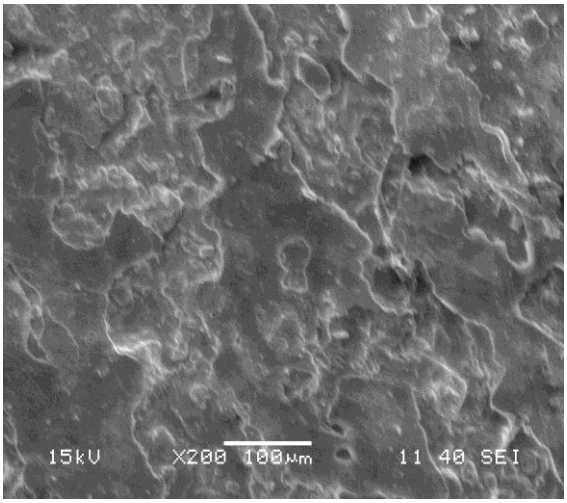

(d)

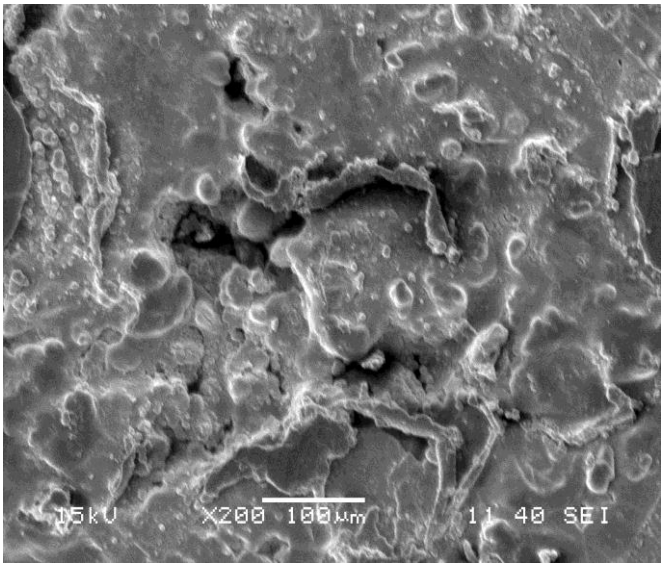

(e)

Fig. 4.12: SEM micrographs of the corroded surfaces corresponding to the (a) Al+Ti; (b) Al+MA; (c) Al+NA; (d) Al+Ti+MA and (e) Al+Ti+NA

In order to examine the morphology of the corroded surface and to understand the mechanism of corrosion, a detailed analysis of the microstructure of the corroded surfaces has been carried out. Fig. 4.12 (a-e) show the representative SEM micrographs of the top view of corroded surface of the all the composites. It is apparent from the figures that localized corrosion has occurred over the whole surface area. The film on the Al+Ti composite is thin, uniform and obviously dense; however, the other composites exhibit thick but irregular and loose films. The corrosion product (most probably Al_2O_3) layer formed on the Al+Ti composite surface is more stable as compared to that on the surfaces of other composites. Thus, the passive film formation on the Al+Ti specimen surface is uniform and film density appears to be improved. In the Al+Ti+MA composite the surface appears to be most degraded than that of the other composites. The discontinuous corroded film with a large size of pits may be noted on the surface of it. However, the film is relatively continuous and less number of small size pits is present on the corroded surfaces of other composites.

4.8.3. Reasons for difference in corrosion behaviour

The microstructural changes introduced by the addition of the particles are the most likely reasons for the difference in corrosion resistance among the composites. Firstly, it is reported that the microstructural refinement provides a superior corrosion resistance [53]. Therefore, the observed grain refinement in the Al+NA and Al+Ti+NA composites may contributes to the improved corrosion resistance.The second possible reasons for the dramatically reduced corrosion resistance with the addition of ceramic reinforcements to the Al matrix could be galvanic coupling between matrix and Al_2O_3 particles. Galvanic coupling might be possible at a first glance, as there is a rather large potential difference between the Al matrix and the Al_2O_3 particles. Based on the polarization measurements and the mix potential theory, Tawari et al. [54] concluded that galvanic corrosion does not play a major role in the corrosion process of Mg/SiC composites. A similar behaviour can be expected for the Al_2O_3particles, although no data is available. The specific electrical resistance of $Al_2O_3 > 10^{14}\Omega$cm appears to be too high to allow effective electron transport and discharge of hydrogen at the reinforcements. Latter is an important part of the corrosion reaction leading to the dissolution of Al. Furthermore, the particles can be considered as defects in the passive film. Thus, it is difficult to build a dense passive layer free from defects in case of composites reinforced with higher volume fraction of ceramic and metallic particles. All the above features are detrimental and may cause difference in corrosion resistance among the composites although it is not possible to separate them. Therefore, it is not known exactly if only one, two or all the above mentioned mechanisms are effective in reducing the corrosion rate.

Chapter 5

Conclusions

5.1. Conclusions

In the present investigation, the combined Ti (micro) and Al_2O_3 (micro or nano) particles reinforced commercially pure Al matrix composites have been developed via powder metallurgy route. A detailed microstructural characterization and the evaluation of mechanical properties including wear and corrosion behaviour have been carried out. As a basis for comparison, the same has been investigated for the Al composites reinforced with these particles alone. The various combinations were Al+8%Ti (Al+Ti), Al+8%micro-Al_2O_3 (Al+MA), Al+8%nano-Al_2O_3 (Al+NA), Al+8%Ti+8%micro-Al_2O_3 (Al+Ti+MA) and Al+8%Ti+8%nano-Al_2O_3 (Al+Ti+MA) (all vol.%). Following are the conclusions arising out of the present study.

1. The composites reinforced with the ceramic particles (micro or nano) alone exhibited higher hardness values as compared to the composite reinforced with metallic particles alone. In addition, the composites reinforced with the nano-sized Al_2O_3 particles alone exhibited higher hardness value as compared to the composite reinforced with the micro-sized Al_2O_3 particles alone. Further the hybrid composites Al+Ti+MA and Al+Ti+NA exhibited a relatively higher hardness values and the same was higher for the later composite. The increase in hardness might be owing to the grain refinement observed in the Al+NA and Al+Ti+NA composites.
2. The stress values sustained by all the composites specimens in compression tests during 50% reduction of their initial height exhibited a similar trend as hardness.
3. The hybrid composites exhibit a better wear resistance than the composite reinforced with individuals particles owing to their higher hardness as compared to that of the

other composites. The dominant wear mechanism is observed to be delamination for the Al+Ti composite and abrasion for the rest of the composites.

4. The Al+Ti composite exhibited the lowest corrosion rate. The composites reinforced with the ceramic particles alone exhibited higher corrosion rate as compared to the Al+Ti composite. In addition, the Al+NA composites exhibited better corrosion resistance as compared to the Al+MA composite. Further relatively higher corrosion rates were exhibited by the hybrid composites. Again the Al+Ti+NA exhibited superior corrosion resistance as compared to that of the Al+Ti+MA. The observed grain refinement in the Al+NA and Al+Ti+NA composites might have contributed to the improved corrosion resistance. Furthermore, the particles can be considered as defects in the passive film. Thus, it is difficult to build a dense passive layer free from defects in case of the composites reinforced with higher volume fraction of ceramic and metallic particles. All the above features are detrimental and may cause difference in corrosion resistance among the composites.

References

[1] Miller WS, Humphreys FJ. Scr Metall Mater 25 (1991) 33.

[2] Lloyd DJ. Int Mater Rev 34 (1994) 1.

[3] Arsenault RJ, Wang L, Feng CR. Acta Metall Mater 39(1991) 47.

[4] Pramila Bai BN, Ramashesh BS, Surappa MK. Wear 15 (1992) 295.

[5] Kwok JKM, Lim SC. Comp Sci Tech 59 (1999) 55.

[6] ASM metals handbook, casting, ASM International, Metals Park, Ohio. 1988: p. 44073.

[7] Fridlyander JN, editor. Metal matrix composites, London: Chapman & Hall, (1995): p. 51.

[8] Midling OT, Grong O. Key Eng Mater 104 (1995) 329.

[9] Everette RK, Arsenault RJ, editors. Metal matrix composites: processing and interfaces, Academic Press, Inc. (1991).

[10] Akio K, Atsushi O, Toshiro K, Hiroyuki T. J Jpn Inst Light Metals 49 (1999) 149.

[11] Thakur SK, Gupta M. Composites: Part A 38 (2007) 1010.

[12] Perez P, Garces G, Adeva P. Comp Sci Tech 64 (2004) 145.

[13] Hassan SF, Gupta M. J Alloys Compd 345 (2002) 246.

[14] Hassan SF, Gupta M. Mater Res Bull 37 (2002) 377.

[15] Hwang S, Nishimura C, McCormick PG. Scr Mater 44 (2001) 2457.

[16] Lu L, Lai MO, Toh YH, Froyen L. Mater Sci Eng A 334 (2002) 163.

[17] Hassan SF, Gupta M. J Alloys Compd, 35 (2002) 10.

[18] Miracle DB. Comp Sci Tech 65 (2005) 2526.

[19] Surappa MK. Sadhana, 28 (2003) 319.

[20] Yadav D, Bauri R. Mater Sci Eng A 528 (2011) 1326.

[21] Yadav D, Bauri R. Mater Let 64 (2010) 664.

[22] Torralba JM, da Costa CE, Velasco F. J Mater Proc Tech 133 (2003) 203.

[23] Bonollo F, Ceschini L, Garagnani GL. App Comp Mater 4 (1997) 173.

[24] Das T, Munroe PR, Bandyopadhyay S. J Mater Sci 31 (1996) 5351.

[25] Lieblich M, Gonza´lez-Carrasco JL, Caruana G. Intermetallics, 5 (1997) 515.

[26] Costa CE, Ph.D. Thesis (1998), Universidad Polite´cnica de Madrid, Spain.

[27] Rana RS, Purohit R, Das S. Int J Sci Eng Res 3 (2012)

[28] Torralba JM, da Costa CE, Velasco F. J Mater Proc Tech 133 (2003) 203.

[29] Hassan SF, Gupta M. J Alloys Compd 345 (2002) 246.

[30] Hassan SF, Gupta M. J Mater Sci 37 (2002) 2467.

[31] Wong WLE, Gupta M. Comp Sci Tech 67 (2007) 1541.

[32] Thakur SK, Gupta M. Comp Part A 38 (2007) 1010.

[33] Raghunath BK, Karthikeyan R, Ganesan G, Gupta M. Mater Des 29 (2008) 622.

[34] Paramsothy M, Srikanth N, Gupta M. J Alloys Compd 461 (2008) 200.

[35] Wu Q, Yang C, Xue F, Sun Y. Mater Des 32 (2011) 4999.

[36] Wang H et al. In situ fabrication and microstructure of Al_2O_3 particles reinforced aluminium matrix composites, Mater Sci Eng A 527 (2010) 2881.

[37] Mazahery A, Ostadshabani M. J Comp Mater 45 (2011) 2579.

[38] Wong WLE, Karthik S, Gupta M. J Mater Sci 40 (2005) 3395.

[39] Sajjadi SA etal. J Alloys Compd 511 (2012) 226.

[40] Nguyen QB, Gupta M. Proceeding of the 3rd International Conference on Processing Materials for Properties 2008, PMP III; Bangkok; Thailand; 1 (2009) 587-591.

[41] Nguyen QB, Gupta M. Mater Sci Eng A 527 (2010) 1411.

[42] Nguyen QB, Gupta M. J Alloys Compd 490 (2010) 382.

[43] Majumdar A, Muddle BC. Mater Sci Eng A 169 (1993) 135.

[44] Zhang Z, Tremblay R, Dube D. Mater Sci Eng A 385 (2004) 286.

[45] Ho KF, Gupta M, Srivatsan TS. Mater Sci Eng A 369 (2004) 302.

[46] Hassan SF, Gupta M. Mater Sci Tech 19 (2003) 253.

[47] Nguyen QB, Gupta M, Comp Sci Tech 68 (2008) 2185.

[48] Suh NP. Wear 44 (1977) 1.

[49] How HC, Baker TN. Wear 232 (1999) 106.

[50] Sahin Y. Wear 223 (1998) 173.

[51] Hosking FM etal., J Mater Sci 17 (1982) 477.

[52] Rohatgi PK etal. Int J Aerospace Innovations 3 (2011) 153-162

[53] Mondal AK etal., Surf Coat Tech 202 (2008) 3187-3198

[54] Tiwari S, Balasubramaniam R, Gupta M., Corr Sci 49 (2007) 711-725